January 2015

Tissue Engineering The Neural Retina With Human Embryonic Stem Cells: Exploring The Role Of The Retinal Pigment Epithelium

Yu Cheng Peter Zhao
Yale School of Medicine, peterzhao8@gmail.com

Tissue engineering the neural retina with human embryonic stem cells: exploring the role of the retinal pigment epithelium

A Thesis Submitted to the

Yale University School of Medicine

in Partial Fulfillment of the Requirements for the

Degree of Doctor of Medicine

Yu Cheng Peter Zhao

2015

Table of Contents

Abstract

In order to restore vision in the late stages of retinal degeneration, it is necessary to address loss of cells from both the retinal pigment epithelium (RPE) and the neural retina. As a step towards generating neural retinal tissue for translational studies, we evaluated a biodegradable polymer scaffold as a three-dimensional vehicle for the directed differentiation of H9 human embryonic stem cells (H9-hESC) into neural retina. Polymer scaffolds were electrospun from 14% w/v polycaprolactone (PCL), approximated the thickness of native neural retina, and consisted of loose, randomly oriented fibers of subcellular diameter. H9-hESC were seeded to PCL scaffolds, cultured in retinal differentiation media, and compared by immunofluorescence and quantitative real-time RT-PCR (qRT^2-PCR) to H9-hESC differentiated on porous Transwell filters. H9-hESC cultured on PCL scaffolds migrated up to 40 microns into the scaffold and expressed markers consistent with cellular proliferation and differentiation into neural retina. Cultures on PCL scaffolds showed equivalent or increased expression of neural retinal markers compared to those grown on Transwell filters. We then co-cultured H9-hESC differentiated on PCL scaffolds with monolayers of RPE and found that each tissue affects the other's maturation. Co-cultured neural retina expressed higher levels of retinal maturation markers, and the transepithelial resistance (TER) of co-cultured RPE was more consistent with physiologic values. Finally, we found that TRP channels expressed in RPE localize to various subdomains of the RPE apical membrane, where they potentially mediate RPE-retinal interactions by sensing the ionic composition of the subretinal space.

Acknowledgements

I would like to thank Dr. Lawrence Rizzolo and Dr. Ron Adelman for their incredible support and enthusiasm over the course of my year in the laboratory. They have been inspiring and insightful mentors, challenging me to continually develop my skills as a scientist and as a clinician. I would also like to thank the other members of the Rizzolo laboratory. Dr. Shaomin Peng, thank you for patiently teaching me many laboratory skills and techniques throughout the year. Dr. Geliang Gan, thank you for your contributions to the TRP channel project and your guidance regarding other TRP channel experiments. Katherine Davis, thank you for being a kind, supportive, and engaging lab-mate and for always offering to help. Lastly I would also like to thank Dr. Lilangi Ediriwickrema for laying the groundwork for this project through her work on electrospinning.

I thank Jason Thomson, Yinghong Ma, and Caihong Qiu at the Yale Stem Cell Core for their expertise, patience, and insightful discussions. Thank you to Aaron Morris and Nina Kristofik for help with the electrospinning apparatus, and for suggestions on optimizing electrospinning parameters. I would also like to thank Dr. John Forrest, Donna Carranzo, and Mae Geter at the Office of Student Research for their support of my work and of student research in general. Because of you all, Yale remains a truly special place for medical students. This work was funded by the National Institutes of Health through the CTSA-TL1 grant.

Finally, I thank my parents, Wei Zhao and Hong Zhu, and my sister Renee Zhao for their love and encouragement throughout my life. I am very grateful for my parents' sacrifices and I would otherwise not be here today.

Introduction

Since the creation of the first cultured human embryonic stem cell (hESC) lines in 1998, scientists and clinicians have been researching regenerative therapies with the potential to restore organ function. Many medical treatments today are aimed at slowing progression or managing symptoms of a chronic process such as cirrhotic liver disease, dementia, or macular degeneration. Regenerative therapies therefore have the potential to fundamentally change medicine's capacity for healing. In 2007, progress in the field was accelerated by the discovery that four transcription factors (Oct4, Sox2, cMyc, and Klf4) could be used to reprogram an individual's somatic cells to a pluripotent state [1]. This discovery made it possible to create all types of new tissues from a patient's own cells, circumventing issues of immunologic rejection.

The eye is a promising site for early trials of regenerative therapies because of its surgical accessibility and the ease of noninvasive monitoring through fundus photography. One part of the eye that stands to benefit from stem cell therapies is the retina, a thin photosensitive tissue that lines on the inner surface of the eye wall (Figure 1). The retina is responsible for the conversion of light into electrical signals that are communicated through the optic nerve to the brain and interpreted as vision. On its apical side, the retina contacts the vitreous humor within the vitreous cavity. On its basolateral side, the retina contacts the choroid and its extensive network of blood vessels, the choriocapillaris. The retina itself is composed of two interdependent tissues: a laminated, multilayered neural retina containing photoreceptors and many other types of neurons, and a monolayer of pigmented supporting tissue called the retinal pigment epithelium (RPE).

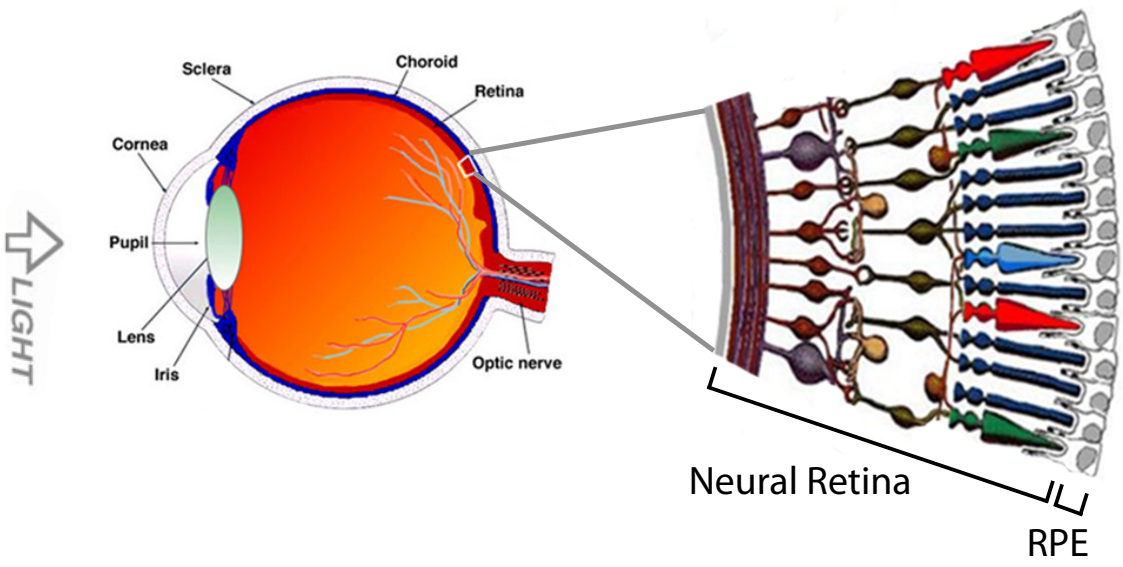

Figure 1. Anatomy of the eye and retina. Light enters the eye, passes through the pupil, and is focused by the lens onto the retina where phototransduction occurs. Neuronal signals are processed and integrated by retinal neurons and then passed along ganglion cell nerve fibers through the optic nerve to the brain. Excess light is absorbed by the retinal pigment epithelium (RPE). Image adapted from Webvision, University of Utah.

Degenerative diseases of the retina are a debilitating cause of irreversible blindness worldwide with few medical therapies available. There are many clinical causes of retinal degeneration including age-related macular degeneration, retinitis pigmentosa, Stargardt's disease, paraneoplastic autoimmune retinopathies, and mitochondrial disease-associated retinopathies such as Kearns-Sayre syndrome.

Age-related macular degeneration (AMD) is the most common retinal degeneration and the leading cause of vision loss in adults over age 55 in developed countries. AMD is an acquired disease that affects over 2 million people in the United States alone, and it is projected to affect more than 3 million by 2020 [2]. Degeneration occurs specifically at the *macula lutea* of the retina. The macula is a densely pigmented area of the central retina that contains the fovea, a zone

specialized for high acuity vision with a high density of cone photoreceptors. The degeneration that occurs in AMD specifically disrupts this central vision which is needed for driving, reading, and recognizing faces. Patients with AMD are fully aware of their central visual loss and become progressively more dependent on others to complete activities of daily living. Unfortunately, the elderly are less able to adjust to the lifestyle changes necessary due to progression of disease. Among affected patients with 20/60 vision or worse one-third have depression, double the baseline rate in those over age 65 [3].

Figure 2. *Left*, normal retina showing the optic disc on the right and the pigmented macula at the center. *Center*, dry AMD is characterized by accumulation of yellow debris called drusen in the macula. *Right*, advanced dry AMD (central geographic atrophy) results from death of sub-macular RPE. The underlying vessels of the choriocapillaris become visible after loss of the pigment-containing RPE. Images courtesy of Webvision/University of Utah, Wikipedia, and Columbia University.

There are two forms of AMD, an atrophic dry form and an exudative wet form. In the more common dry form, cellular debris called drusen accumulate between the retina and the choroid, causing chronic inflammation and interfering with nutrient and oxygen exchange. In a subset of patients with dry AMD, the diseased retina increases expression of vascular endothelial growth factor (VEGF), causing new blood vessels to grow into the retina from the choriocapillaris. These new vessels are leaky and

friable, leading to macular edema, hemorrhage, and scarring. Over the past decade, exudative AMD has become a treatable disease with the invention of the intravitreal anti-VEGF agents bevacizumab (Avastin), ranibizumab (Lucentis) and Eylea (aflibercept) to counteract angiogenesis [4, 5]. In contrast, there remain no proven medical or surgical treatments for advanced dry AMD, otherwise known as central geographic atrophy (CGA). For example, although the AREDS2 trial demonstrated that a daily vitamin formulation had some efficacy for preventing progression of early dry AMD to exudative AMD, the trial showed no efficacy in preventing progression of early dry AMD to CGA in primary or subgroup analyses [6]. CGA is becoming responsible for a significant proportion of AMD-associated blindness and remains unpreventable and untreatable.

The cellular and molecular mechanisms of retinal degeneration are complex and multifaceted, but a common feature is atrophy of the RPE. This monolayer of pigmented cells extends microvilli in the subretinal space to contact photoreceptors on its apical side, and rests on Bruch's membrane and vessels of the choriocapillaris on its basolateral side (see Figure 1). RPE forms the outer blood-retina barrier with its epithelial tight junctions, actively transporting nutrients and metabolic waste products across the barrier. In addition RPE participates in cycling of the visual chromophore retinaldehyde, secretes trophic factors and paracrine signaling molecules, and buffers the ion composition of the subretinal space [7]. RPE and neural retina develop together embryologically, arising from opposite poles of the optic vesicle. By week 24, the optic vesicle lumen collapses into a potential space called the subretinal space, allowing the outer segments of photoreceptors to interdigitate with the apical microvilli

of RPE [8]. In adulthood, separation of the neural retina from the RPE (i.e. retinal detachment) rapidly leads to photoreceptor apoptosis and retinal scar formation, highlighting the crucial role of RPE in sustaining the neural retina [9]. In dry AMD, drusen accumulates between the RPE and Bruch's membrane, leading to loss of RPE and secondary degeneration of the neural retina. On the other hand, primary photoreceptor mutations can cause RPE atrophy. For example, mutations in the ABCA4 transporter protein in photoreceptors can cause accumulation of the toxic metabolite A2E, leading to a juvenile form of macular degeneration called Stargardt's disease [10]. These examples illustrate that derangements in either layer can ultimately affect the function of both tissues, leading to vision loss. Thus the interdependence of the neural retina and RPE is important to consider when evaluating putative pharmacologic agents and stem cell therapies.

Stem cells are a promising approach to regenerating the retina and restoring vision. RPE derived from hESC can be readily generated with high cellular purity. Schwartz, *et al*. are conducting the first clinical trial using hESC-derived RPE, and have reported preliminary results on injecting RPE cells into two patients with late-stage AMD and Stargardt's disease, respectively [11]. The preliminary report showed the graft was safe with no evidence of teratoma formation or immunologic reaction months after the intervention. However, improvement in vision was not clinically significant, highlighting the chief limitation of RPE-only transplantation. The newly introduced RPE is not capable of generating new photoreceptors, so the capacity of RPE-only therapy to restore vision is dependent on the number of viable existing photoreceptors [12]. In the late stages of retinal degeneration, many photoreceptors

have already been irreversibly lost. This limitation is especially important because the experimental nature of stem cell therapy makes intervention during the early stages of degeneration unlikely, since potential risks would heavily outweigh possible benefits. For the foreseeable future, the primary goal of stem cell therapy will remain restoring vision in patients with late stage disease. Therefore, stem cell therapies must be capable of replacing both lost RPE and neural retinal tissue. In contrast to RPE, the generation of functional photoreceptors and retinal neurons with the capacity to integrate into the host retina remains a challenge because the neural retina is a complex, multilayered tissue and its embryogenesis is not fully understood.

What is known is that neural retina develops from self-organizing retinal progenitor cells (RPC). RPCs are multipotent retinal cells, and over subsequent cell divisions give rise to different types of neurons including photoreceptors, amacrine cells, bipolar cells, and ganglion cells. Over the past several years, three-dimensional culture techniques have seen tremendous success in generating neural retina because they use the innate self-organizing drive of RPCs. This improvement over conventional two-dimensional cultures is thought to be because three-dimensional culture models more accurately recreate the cell-to-cell and paracrine interactions of the *in vivo* environment.

There are many techniques for three-dimensional culture including free-floating spheroids, scaffolds, bioreactors, magnetic levitation, and hanging drop culture. Three-dimensional free-floating spheroid cultures have been successful specifically for growing neural retina [13-15]. In this method, hESC are dissociated and re-aggregated into spherical embryoid bodies that are cultured on non-adherent tissue culture plates

in a neural differentiation medium. After several weeks optic cups form on a region of the embryoid bodies, and the optic cup tissue on each embryoid body is manually isolated for further culture and expansion. Unfortunately this method is labor-intensive and difficult to scale up. Presently, large numbers of retinal cells are needed for transplantation studies because of low rates of integration into host tissue. For example, one study of transplantation into a mouse model of retinal degeneration found that only 0.3% of transplanted cells harvested during the optimal embryologic time window survived and integrated into the host retina [14]. Therefore, a more uniform and scalable method of culturing neural retina is needed for human transplantation studies.

One approach to scaling three-dimensional cultures is the use of biodegradable scaffolds as an organizing matrix for cellular attachment, growth, and migration. The Rizzolo lab has developed a method of electrospinning PCL polymers in conjunction with the lab of W. Mark Saltzman (Yale University). PCL is an FDA-approved biodegradable polymer which is superior for retinal applications due to its low retinal toxicity compared to other polymers such as PLLA and PLGA, both of which release lactic acid during degradation [16]. Electrospinning is a scaffold manufacturing process that applies high voltage to a viscous solution of dissolved polymer. As the charged solution is pushed out through a needle tip by a syringe pump, it forms a Taylor cone at the needle tip and becomes a narrow jet. The jet solvent evaporates during flight from the syringe tip to the collecting apparatus, forming a polymer fiber.

Scaffolds constructed from materials including PCL have been shown to improve the adherence, survival, and maturity of RPC and RPE both *in vitro* and when

transplanted into mouse models [17-20]. Another advantage of scaffolding is that it can be coated with extracellular matrix proteins. For example, one study showed that between extracellular matrix proteins and growth factors in the reagent Matrigel, the extracellular matrix proteins including laminin and collagen were more important for stimulating neural retinal differentiation [21]. This model is consistent with our understanding of *in vivo* development, in which the neural retina and RPE develop between the vitreoretinal interface and Bruch's membrane, both of which are composed of laminin, fibronectin, and collagen [8].

Another advantage of using a biodegradable polymer scaffold for three-dimensional culture is the ability to co-culture the neural retina grown on the scaffold with a monolayer of RPE. Neural retina and RPE are interdependent during embryologic development and recapitulating their interdependence *in vitro* may help further tissue maturity. The interdependence of the RPE and the neural retina is illustrated in animal models of retinal transplantation, which show that successful transplantation of RPE or neural retinal precursors is reported only when transplant is performed before the degeneration of photoreceptors begins [12, 22, 23]. Radtke *et al*. demonstrated that transplant of an RPE-neural retina fetal explant had superior outcomes over transplant of either tissue alone [24]. In addition, McUsic *et al*. showed that RPE promotes the formation of outer segment-like projections in photoreceptor precursors [25]. Outer segments are photoreceptor appendages that contain high concentrations of sensory pigments such as rhodopsin and opsin, and the presence of outer segments that rhythmically shed membranous discs is a necessary marker for functional maturity. Studies in mice have shown that a high degree of terminal

differentiation is necessary to form structures that resemble outer segments, but that terminal differentiation alone may not be sufficient to form functional outer segments [26, 27].

Conversely, the RPE may also require the neural retina for further maturation, and co-culture will help explore this hypothesis. The Rizzolo lab replicated published data on producing hESC-RPE, and found that a serum-free medium (SFM-1) stabilizes and increases the transepithelial resistance (TER), a well-established marker of RPE barrier function. This outcome suggested that SFM-1 promotes physiologic functioning of RPE tight junction proteins and ion transporters [28]. Using RNA sequencing, a panel of 25 RPE genes was found to be over- or under-expressed in hESC-RPE compared to 16-week human fetal RPE (hfRPE), suggesting that hESC-RPE is gestationally "younger" than 16-week RPE and could benefit from interactions with neural retina.

The characterization of RPE-neural retina co-culture also led us to examine transient receptor potential (TRP) channels, a superfamily of ion channels known to activate in response to mechanical, thermal, and chemical fluctuations in the local tissue environment. Different TRP channels are differentially permeable to cations including Na^{+}, Mg^{2+}, and Ca^{2+}. Because many functions of RPE support the metabolic activities of the neural retina, we explored whether TRP channels might play a role in modulating these RPE functions, which include sensing and maintaining the ion composition of the subretinal space and transporting water from the subretinal space to the choriocapillaris.

Note: the discussions on TRP channels follow a manuscript in press in the journal *Investigative Ophthalmology and Visual Science* (Zhao PY, Gan G, Peng S, Wang S, Chen B, Adelman RA, Rizzolo LJ. TRP channels localize to subdomains of the apical plasma membrane in human fetal retinal pigment epithelium.)

Statement of Purpose

Retinal degenerations including age-related macular degeneration are a common cause of blindness in the developed world and new therapies are needed. Early human trials with stem cell-derived RPE demonstrate clinical safety but not clinical efficacy, in large part because the photoreceptors and neurons lost in the late stages of degeneration remain difficult to consistently generate *in vitro*. The objective of this study is to evaluate a biodegradable polycaprolactone scaffold for its ability to support three-dimensional culture specifically for neural retinal cells including photoreceptors and neurons, and to establish a preliminary co-culture of neural retinal cells and RPE. This study also seeks to better understand interactions between neural retina and RPE by exploring the expression pattern and function of TRP channels in RPE. A successful *in vitro* co-culture model could be used as a platform to understand how the neural retina and RPE together respond to environmental perturbations, and as a precursor towards successful co-transplantation of neural retina and RPE to regenerate tissue and restore vision in degenerative retinal diseases.

Specific Aims

Aim 1: Evaluate the maturity and tissue architecture of hESC-derived neural retina grown on a three-dimensional scaffold and compare to hESC-derived neural retina grown on conventional two-dimensonal Transwell filters.

Our hypothesis is that PCL scaffolds will provide a three-dimensional environment that supports the directed differentiation of H9-hESC to neural retina to a greater degree than the conventional two-dimensional environment found on Transwell filters. We will establish a consistent protocol for differentiation based on methods described in the literature and use the protocol to compare PCL scaffolds with Transwell filters.

Aim 2: Assess whether hESC-derived neural retina grown on PCL can be induced to further mature by co-culture with RPE.

Our second hypothesis is that co-culturing hESC-derived neural retina with the RPE will induce further maturity in the neural retinal tissue as compared to monoculture. Neural retina and RPE are interdependent tissues, suggesting that cell-to-cell contact and paracrine effects simulated by co-culture could induce neural retina and/or RPE to mature further than they otherwise would in monoculture.

Aim 3: Characterize TRP channels of the RPE and explore their role in regulating RPE function.

The third hypothesis is that since TRP channels are conduits for the entry of divalent cations, we can functionally characterize TRP channels using barium (Ba^{2+})

as a surrogate for calcium (Ca^{2+}). We will use a well-established culture model of human fetal RPE (hfRPE) isolated from 15-16 week gestation fetal eyes [29]. These cultures were highly polarized and possessed functional and electrophysiological properties attributed to native adult human RPE [30, 31]. We will then determine the TRP channel expression profile of hfRPE and show the subcellular localization of TRP channels.

Materials & Methods

Electrospinning & Scanning Electron Microscopy

PCL scaffolds were electrospun from polycaprolactone (Average M_w ~14,000; Sigma-Aldrich) using a protocol adapted from Lilangi Ediriwickrema, a former medical student in the Rizzolo laboratory. Stock polymer beads were dissolved in a solution of chloroform and ethanol (11:1 ratio) to form a viscous 14% w/v polymer solution. 4 ml of solution was loaded into a 10 ml syringe. The syringe was equipped with a 16 gauge blunt-tip needle and loaded horizontally into the pump apparatus (see Figure 3). A voltage of 20 kV was applied to the needle tip and solution was eluted at a rate of 50 microliters per minute. Fibers were collected on a rotating mandrel forming a sheet of material, and circular scaffolds were cut from the sheet using a punch biopsy tool.

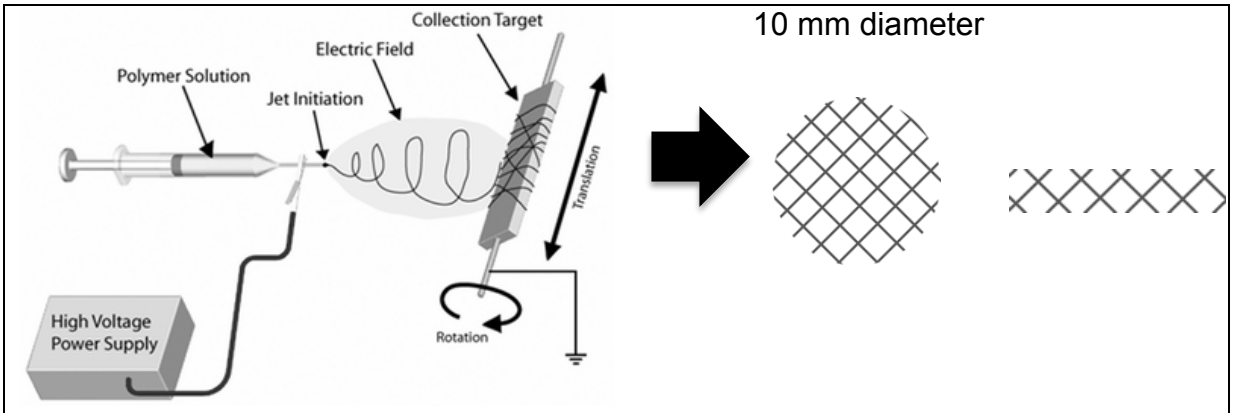

Figure 3. Schematic of electrospinning setup. A punch biopsy tool was used to create 10 mm circular scaffolds from the spun PCL sheet. Image adapted from Sell SA, Bowlin GL, *J. Mater. Chem.* 2008 18, 260-263.

Scanning electron microscopy was used to evaluate scaffold microarchitecture. Scaffolds were mounted in a Denton vacuum chamber and sputter-coated with 10 nanometers of amorphous chromium. Images were captured using a Hitachi SU-70 (Yale Institute for Nanoscience and Quantum Engineering) with 10kV acceleration voltage. For *en face* imaging, scaffolds were soaked in ethanol, frozen with liquid nitrogen, and cut with a scalpel blade. Scaffolds were then chromium-coated as above and mounted onto a tilted stage for imaging.

Directed Differentiation of H9-hESC on 2D Transwell Filters & 3D PCL Scaffolds

Research adhered to the principles of the Declaration of Helsinki. The H9 stem cell line, originally developed at the University of Wisconsin, was maintained and passaged by Jason Thomson, Yinghong Ma, and Caihong Qiu at the Yale Stem Cell hESC/iPSC Core Laboratories. Briefly, frozen vials were thawed to 4°C, plated onto 1% Matrigel (BD Biosciences)-coated dishes, and maintained in mTeSR-1 (Stem Cell Technologies) media. Media was changed every 2 to 3 days, and colonies were

routinely scraped under a microscope to remove spontaneously differentiating cells. For passaging, colonies were lifted enzymatically by incubating with 1 U/ml dispase (Stem Cell Technologies) at 37°C for 30 minutes, triturated, washed with phosphate-buffered saline (PBS), and then plated onto 1% Matrigel-coated dishes. Cells from passages 28-65 were used in subsequent experiments.

H9-hESC were seeded to PCL scaffolds or Transwell filters and differentiated based on modifications of established protocols as follows [21, 32]. Prior to use, H9-hESC colonies were examined microscopically and differentiated cells were scraped and washed away. Colonies were lifted enzymatically by incubating at 37°C with 1 U/ml dispase for 30 minutes. Colonies were washed three times with DMEM/F12 (Life Technologies), spun at 500 rpm, and then triturated 5-7 times in a 15 ml tube to reduce colony size to 100-200 microns. PCL scaffolds were sterilized with 100% ethanol for 20 minutes, washed three times with PBS, and coated with 2% w/v Matrigel dissolved in DMEM/F12. Transwell filters (Corning) were 12 mm in diameter and were designed with 0.4 micron pores for permeability between the apical and basolateral culture chambers. Transwell filters were also coated with 2% w/v Matrigel in DMEM/F12. Colonies were plated onto coated PCL scaffolds or coated Transwell filters using a pipet tip. Plates were incubated for 1 hour at 37°C to allow for colony adherence, and then N2B27 media composed of 1% N2 supplement (Life Technologies) and 1% B27 supplement (Life Technologies) in DMEM/F12 was added. For the first day or first three days of differentiation, 2% Matrigel was also included in the N2B27 media added to the apical media chamber. Thereafter, N2B27 media without Matrigel was used and the media was changed every 2 to 3 days. Density

optimization experiments were performed to determine the optimal number of colonies to plate per scaffold or filter. Colony densities of 100, 50, 25, and 12 colonies per Transwell were plated and observed for 2 weeks for cell morphology and evidence of cell detachment. Cultures were analyzed by qRT^2-PCR as described under Aim 1 using RNA primers and using the neural retina PCR array (see PCR methods below). Immunofluorescence was performed to assess protein expression of known neural retinal markers (Pax6, Crx, recoverin, opsin, rhodopsin, Prox1) (see immunofluorescence methods below).

Co-culture of Neural Retina on PCL Scaffolds with Retinal Pigment Epithelium

Two similar varieties of RPE, cultures derived from H9-hESC (H9-RPE) and cultures derived from 16-week human fetal RPE (hfRPE) were prepared for co-culture experiments. In prior work, these varieties were determined to have different maturity levels, which might modulate the effects of co-culturing [28].

H9-RPE was differentiated by the Idelson protocol [33]. Briefly, H9-hESC maintained as described above were lifted by incubating in 1 U/ml dispase for 30 minutes at 37°C, washed three times with DMEM/F12, and then transferred to low-adherence tissue culture plates and maintained as floating embryoid bodies for 1 week in 14% knockout serum replacement (KSR) media. Embryoid bodies were transferred to 1% Matrigel-coated tissue culture plates and maintained in KSR media. After 2 weeks of culture, pigmented cells appeared and were manually selected by scraping and removing non-pigmented and non-polygonal cells. After 1 month of culture, H9-RPE was trypsinized and reseeded to mouse laminin (BD Biosciences)-

coated Transwell filters. After confluence, cells were adapted to SFM-1 media containing 70% DMEM, 30% F12, 2% B27 supplement, and 1% antibiotic-antimycotic solution (Invitrogen) [34].

Primary cultures of hfRPE were obtained from Sheldon Miller (National Eye Institute). Cultures were trypsinized and reseeded on 0.4 micron pore Transwell filters coated with 5% human extracellular matrix (BD Biosciences). After reseeding, cultures were maintained for 4 weeks in media containing 5% serum as previously described [31]. After cultures became confluent and the TER stabilized, they were adapted to SFM-1 as described above. Cultures were maintained in SFM for at least 1 month prior to experiments.

The functional maturity of H9-RPE and hfRPE cultures was monitored over time using transepithelial electrical resistance (TER). An EVOM resistance meter was attached to a chamber containing Endohm electrodes (World Precision Instruments). The chamber was sterilized with 100% ethanol for 30 minutes and washed three times with DMEM/F12 media prior to use. The chamber was filled with DMEM/F12 warmed to 37°C and Transwell inserts were transferred and measured. When the TER of cultures stabilized, the media was changed from SFM-1 to N2B27, and the TER was followed for an additional 1 month. Cultures were analyzed by immunofluorescence for expression and subcellular distribution of paracingulin and Otx2.

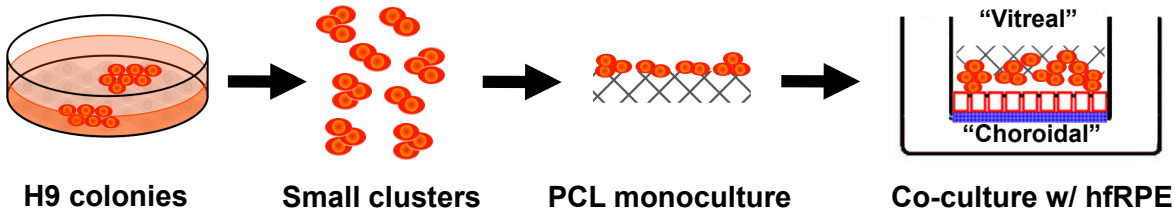

Figure 4. Diagram of the co-culture method. H9-hESC colonies were lifted, gently triturated to reduce size, and plated on Matrigel-coated PCL scaffold (orange circles). After 2-4 weeks of monoculture, scaffolds were mechanically transferred and flipped to rest on a monolayer of RPE (red squares) grown on porous Transwell inserts (blue). Both apical (vitreal) and basolateral (choroidal) chambers contained N2B27 media.

After neural retina was differentiated on PCL scaffolds for 2-4 weeks, co-cultures were formed as illustrated in Figure 4. Co-cultures were maintained for 1 month and during this period the TER was monitored. After 1 month, the PCL scaffold containing neural retina was manually separated from RPE and the two tissues were separately analyzed by immunofluorescence and qRT^2-PCR (see below).

Maturity of the RPE layer was assessed by qRT^2-PCR. The Rizzolo lab has compared the transcriptome of hESC-RPE derived from two hESC cell lines and 16-week hfRPE. 25 genes were selected from RPE signature genes and genes related to RPE barrier function. These 25 genes were identified as statistically over- or under-expressed more than fourfold in hESC-RPE relative to hfRPE. A PCR array was created with these genes in partnership with Biorad. This array was used to compare the transcriptome of co-cultured RPE and monocultured RPE.

Immunofluorescence Confocal Microscopy

Tissue and subcellular distribution of retinal markers was determined by indirect immunofluorescence. Samples were washed twice with cold PBS, fixed with 4%

paraformaldehyde at room temperature for 20 minutes, and permeabilized with 0.1% Triton X-100. When staining for TRP channels, fixation was performed with ice-cold 100% ethanol instead of paraformaldehyde and the permeabilization step was omitted, with all other steps performed identically. After three PBS washes, samples were blocked with 5% donkey serum and 1% BSA in PBS for 1 hour. After incubation with primary antibody overnight at 4°C, samples were washed three times in PBS and incubated with secondary antibody at room temperature for 1 hour.

Primary antibodies were selected from the literature based on their use as retinal markers validated in previous studies and in the Rizzolo laboratory [13, 15, 21, 35]. Rabbit anti-Ki67 (1:300, Thermo Scientific) is an antibody raised against a nuclear protein associated with cellular proliferation. Rabbit anti-Pax6 (1:300, Covance), goat anti-Vsx2 (1:100, Santa Cruz Biotechnology), biotinylated anti-Otx2 (1:100, Invitrogen), and mouse anti-Crx (1:200, Sigma-Aldrich) are antibodies to eye field transcription factors corresponding to the beginning of neural retinal development (Pax6), intermediate development (Vsx2, Otx2), and late differentiation to photoreceptor precursors (Crx). Rabbit anti-Prox1 (1:200, Sigma-Aldrich), rabbit anti-recoverin (1:300, Millipore), rabbit anti-S-opsin (1:200, Santa Cruz Biotechnology), and mouse anti-rhodopsin (1:200, Sigma-Aldrich) are antibodies to proteins present in functional neural retina corresponding to retinal interneurons (Prox1) and photoreceptors (recoverin, S-opsin, rhodopsin). For TRP channel studies, primary antibodies were selected to TRP channels with the most highly expressed mRNAs: rabbit anti-TRPC1 (1:300, Thermo Scientific), rabbit anti-TRPC4 (1:200, Thermo Scientific), rabbit anti-TRPM1 (1:500, Sigma-Aldrich), rabbit anti-TRPM3 (1:800,

Abcam), rabbit anti-TRPM7 (1:1000, Abcam), and rabbit anti-TRPV4 (1:300, Alomone Laboratories). The integrity of RPE tight junctions was assessed with rabbit anti-paracingulin (1:300, Santa Cruz Biotechnology) and mouse anti-ZO-1 (1:200, Invitrogen), and the locations of the RPE primary cilium and basal body were respectively determined with goat anti-gamma tubulin (1:150, Santa Cruz Biotechnology) and mouse anti-acetylated tubulin (1:1000, Sigma-Aldrich). Subcellular localization of the protease m-calpain was evaluated using goat anti-calpain2 (1:150, Santa Cruz Biotechnology). Secondary antibodies (Jackson ImmunoResearch) were used at 1:200 dilution and included: donkey anti-rabbit Cy2, donkey anti-goat Cy3, donkey anti-mouse Cy5, donkey anti-mouse Cy3, and streptavidin-conjugated Cy3. Nuclear staining was performed with 4',6-diamidino-2-phenylindole (DAPI, Sigma-Aldrich). After DAPI staining, three additional PBS washes were performed, samples were mounted to slides with ProLong Gold AntiFade (Life Technologies), and slides were cured overnight. Fluorescent channels were captured in grayscale using an LSM 410 Yokogawa spinning-disc confocal microscope and then processed and colorized with the AxioVision or Zen software suites (Carl Zeiss).

Quantitative Real-time RT-PCR

Total RNA was extracted using the RNeasy Mini kit (Qiagen). cDNA was reverse transcribed from 2 μg total RNA using the QuantiTect Reverse Transcription Kit (Qiagen). Expression analysis of individual genes was performed using iTaq SYBR Green (Biorad) and RNA primers generated at the Keck Oligonucleotide Synthesis Facility (Yale University). In addition, cultures were analyzed using a customized PCR

array (Biorad) for 48 genes involved in neural retinal development and terminal differentiation to photoreceptors, ganglion cells, interneurons, and interneurons (see Figure 10). Relative mRNA expression was calculated using the $2^{-\Delta\Delta Ct}$ method and normalizing to GAPDH. All reactions were performed in triplicate.

Co-culture data were compared to control monocultures of neural retina differentiation on PCL scaffolds and RPE on Transwell filters. A higher degree of maturity in co-culture would support the theory that RPC and RPE are interdependent both in embryological development and physiologic function.

Barium and Calcium Studies for TRP Channels

hfRPE used for TRP channel experiments was prepared identically as hfRPE for co-culture experiments (see above), except that the cultures were maintained in SFM-1 and not adapted to N2B27. Experiments were performed by exchanging half of the SFM-1 in Transwell chambers with 2X concentrations of $BaCl_2$ or $CaCl_2$ and inhibitors or ionophores diluted in SFM-1. Inhibitors were first dissolved in dimethyl sulfoxide (DMSO) (AmericanBio) to create a stock solution and then diluted to the indicated concentrations on the day of the experiment (DMSO < 1% of total media). The peptide inhibitor caloxin 1b1 (Anaspec, Inc) was dissolved directly in SFM-1. Final concentrations were: 3.0 mM $BaCl_2$ (Thermo Scientific), 6.3 mM $CaCl_2$ (Sigma-Aldrich), 2.0 mM $LaCl_3$ (Sigma-Aldrich), 5.0 μM valinomycin (R&D Systems), 10 μM nifedipine (Alfa Aesar), 20 μM ML204 (Sigma-Aldrich), 1.0 μM HC-067047 (Sigma-Aldrich), 100 μM ALLM (Santa Cruz Biotechnology), and 400 μM caloxin 1b1. Solutions were added to both apical and basolateral media chambers unless

otherwise specified. After media exchange, tissue culture plates were gently agitated to mix media and incubated at 37°C. TER was measured prior to media exchange and at 2 and 4 hours of incubation.

Immunoblotting

Samples were washed with ice cold PBS and lysed by sonication into a 25 mM Tris (pH 8.0) solution containing protease inhibitor and 1% SDS. 20 µg protein extracts were diluted in Laemmli sample buffer, separated on a 7.5% Tris-HCl polyacrylamide gel (Bio-Rad), and transferred to polyvinylidene fluoride (PVDF) membranes (PerkinElmer Inc). After 1 hour incubation in Membrane Blocking Solution (Life Technologies), membranes were incubated with primary antibodies overnight at 4°C (rabbit anti-TRPC1 1:300, rabbit anti-TRPC4 1:200, rabbit anti-TRPM1 1:500, rabbit anti-TRPM3 1:800, rabbit anti-TRPM7 1:1000, rabbit anti-TRPV4 1:300). Membranes were washed three times with PBS containing 0.2% Tween and incubated with horseradish peroxidase-conjugated donkey anti-rabbit antibodies (1:3000, Thermo Scientific) for 1 hour. After three additional washes, proteins were visualized with SuperSignal West Femto Chemiluminescent Substrate (Thermo Scientific). Images were captured using the ChemiDoc XRS System (Bio-Rad). M_r values were calculated relative to PrecisionPlus Dual Color Standards (Bio-Rad). Immunoblots were performed on at least two distinct cell samples from different primary culture flasks.

Results

Aim 1: Evaluate the maturity and tissue architecture of hESC-derived neural retina grown on a three-dimensional scaffold and compare to hESC-derived neural retina grown in conventional 2D culture.

Electrospun PCL Scaffolds

Scaffolds produced by electrospinning were examined under scanning electron microscopy (Figure 5). Scaffold fibers were randomly oriented and loosely arranged and formed 20-40 micron pores. At 10,000x, a representative scaffold fiber is shown with a fiber diameter of 2 microns. An *en face* view was obtained, in which fibers appear more compact in the z-plane than the x-y plane. The compactness of fibers in the z-plane is likely a consequence of the electrospinning process, which adds fibers in successive layers. Scaffolds were approximately 150 microns thick, comparable to adult retinal thickness of 200 microns at the macula and 300 microns in the peripheral retina.

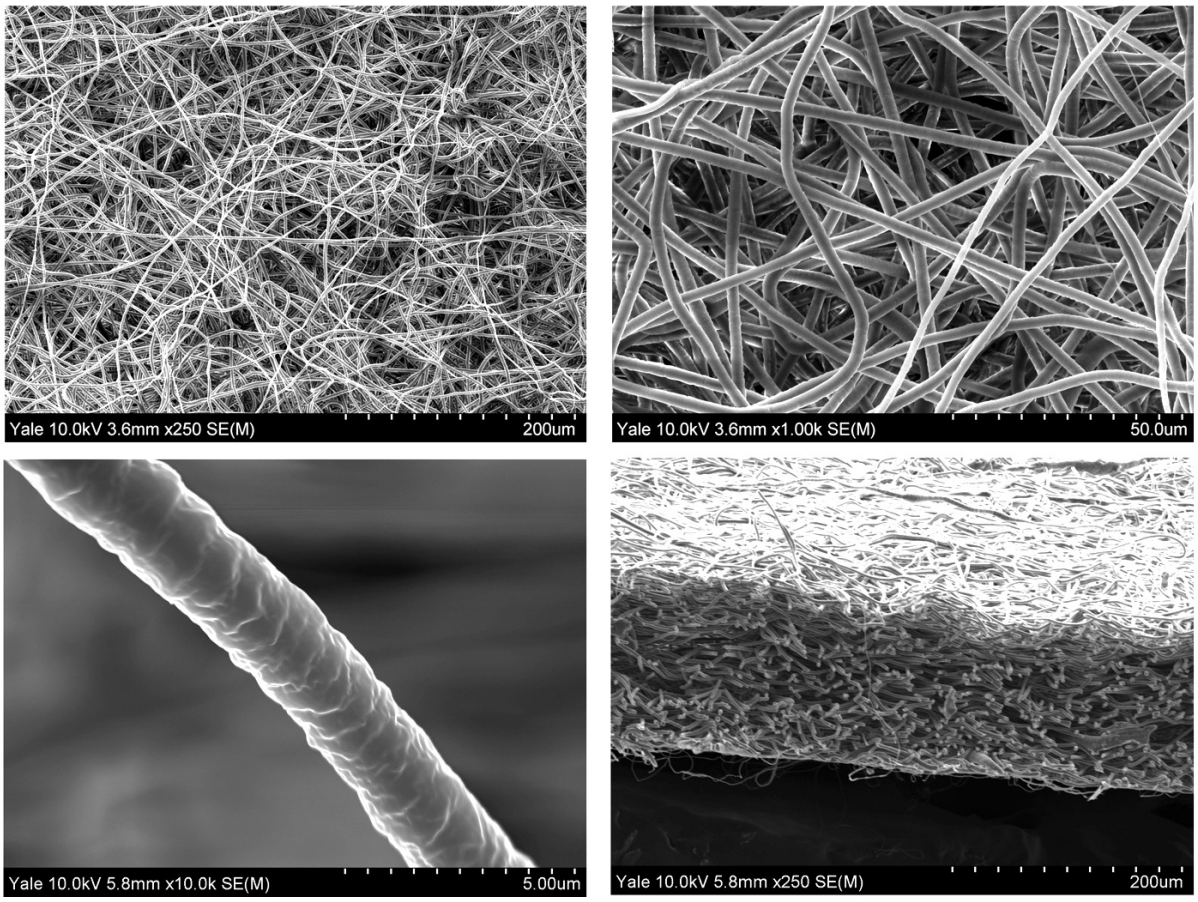

Figure 5. *Top left*, electrospun PCL scaffolds have loosely arranged, randomly oriented fibers. *Top right*, scaffold pores are approximately 20-40 microns in size. *Bottom left*, individual PCL fibers measure 2 microns in diameter. *Bottom right*, en face view reveals scaffolds are 150 microns in thickness and compact in the z-plane.

Differentiation in 2D vs. 3D Culture

H9-hESC were maintained in mTeSR media and manually scraped to remove differentiating colonies. Immediately prior to harvesting cells for directed differentiation, H9 colonies showed typical stem cell colony morphology reflected by a uniform population of cells centrally, and cells with slightly flattened morphology at the colony edges (Figure 6). Colonies ranged from 400 to 1000 microns in diameter at

time of harvesting, and were gently triturated 5-7 times to produce cell clusters 200 microns in diameter.

Two days after seeding, colonies on Transwell filters adopted a rounded morphology and polarized appearance (Figure 6). This polarized appearance was consistent with differentiation towards a transient, self-organizing neuroepithelium, and by day 5 colonies stained positively for the early neuroepithelial marker Pax6. By day 12, the polarized neuroepithelium flattened and expanded forming neural rosettes. For neural retina differentiating on PCL scaffolds, colonies were difficult to visualize due to PCL fibers, but could be identified with light microscopy as opacities present on the scaffolds. The exact morphology of the scaffold-grown colonies could not be monitored over time due to the scaffold's interference with light microscopic imaging.

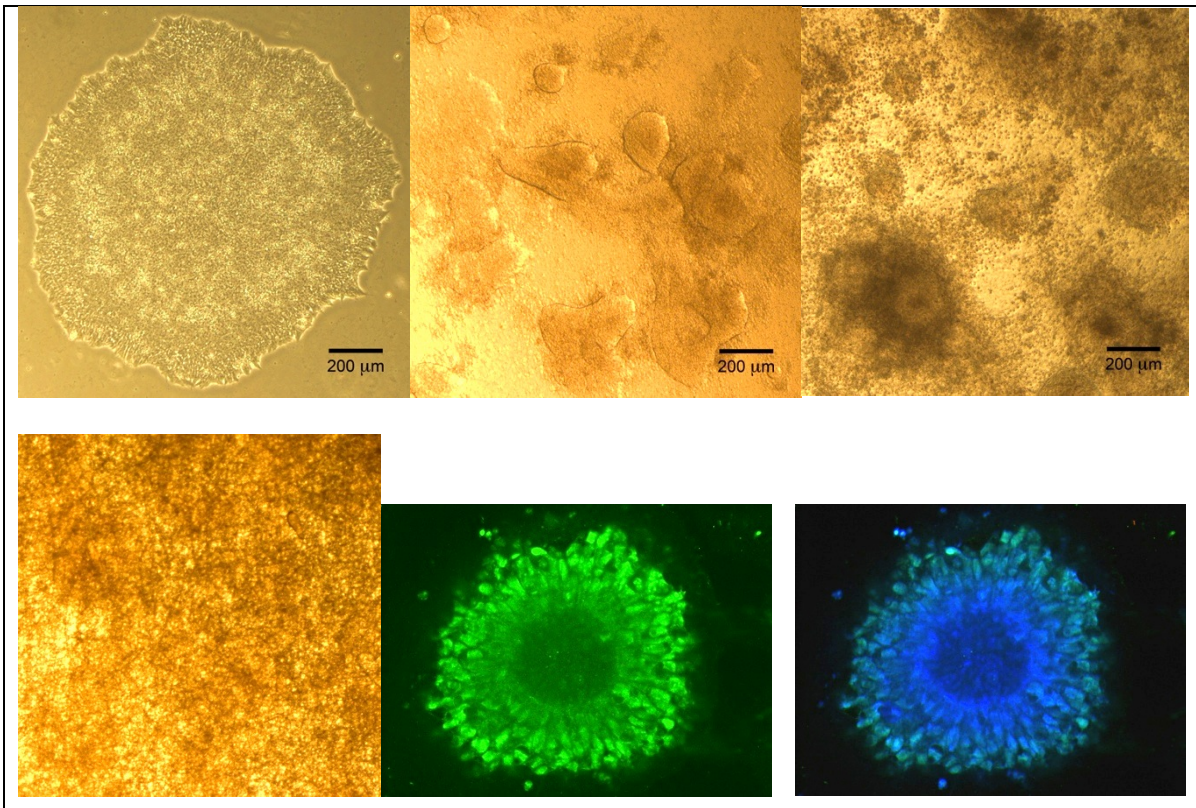

Figure 6. *Top*, From left to right, light microscopic appearance of cells prior to differentiation protocol, on Transwell filters day 2, and on Transwell filters day 14.

Note polarized neuroepithelium present on day 2 and formation of neural rosettes by day 14. *Bottom left*, light microscopic appearance of cells on PCL scaffold as densities. *Bottom center and right*, by day 5 cells grown on Transwell filters form $Pax6^+$ polarized structures (green, Pax6; blue, DAPI)

To determine the optimal seeding density, serial dilutions of H9-hESC colonies were created and plated onto 2% Matrigel-coated Transwell filters, which have a growth surface area of 1 cm^2 (Figure 7). Filters seeded with 100 colonies per Transwell filter experienced significant cell death. Each day the media was exchanged, the pH indicator present in the media indicated highly acidity, suggesting that cell density was too high and leading to rapid metabolism of media nutrients and accumulation of toxic metabolic products. Conversely, Transwell filters seeded with 25 and 12 colonies per Transwell contained areas devoid of cells. A seeding density of 50 colonies per Transwell was optimal and used for all subsequent experiments.

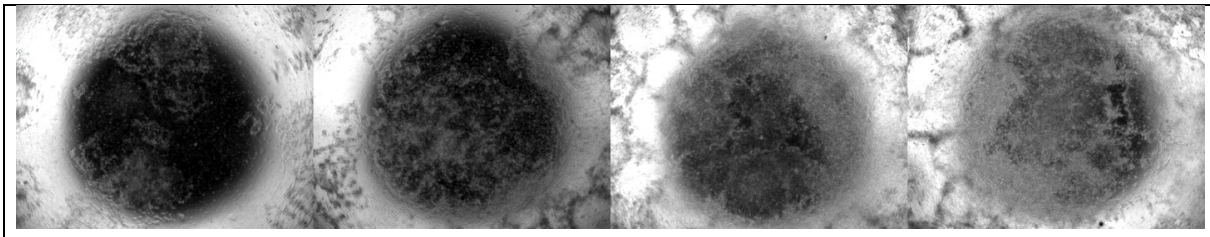

Figure 7. *From left to right*, Transwell filters seeded with 12.5, 25, 50, and 100 H9-hESC colonies per Transwell after 2 weeks of differentiation. In the 100 colonies per Transwell experiment, numerous cells detached from the filter.

After 30 days cultures were more thoroughly analyzed by qRT^2-PCR and immunofluorescence. Cultures grown on Transwell filters downregulated the pluripotency markers Oct4 and Nanog, indicating that cells were successfully induced to differentiate. The mesodermal marker Brachyury was also downregulated, while the endodermal marker Gata4 remained unchanged and at low levels (cycle threshold

~34). The neural retina markers Pax6 and Rax were upregulated. Transcript levels of the retinal progenitor cell marker Vsx2 were 1,000-fold greater in differentiated cells. In the developing retina, Pax6 and Rax are upregulated early, followed by Vsx2 and then Crx. The high levels of Vsx2 present in culture indicate the presence of retinal progenitor cells. In contrast, Otx2 showed minimal change in expression compared to H9 undifferentiated stem cells. Otx2 is a transcription factor first expressed, then downregulated in the neural retina and upregulated in RPE. The lack of change in Otx2 expression might therefore reflect a combination of upregulation and downregulation in different cell subtypes, leading to minimal changes in overall gene expression.

Figure 8. Comparison of gene expression in RPC differentiated on Transwell filters for 30 days, and H9-hESC. Pluripotency markers and mesodermal marker Brachyury were downregulated, while neural retinal markers Pax6 and Rax were upregulated. Vsx2 was highly upregulated and Otx2 was slightly downregulated. Data were obtained from two separate experiments and PCR reactions were performed in triplicate. Error reported as SEM.

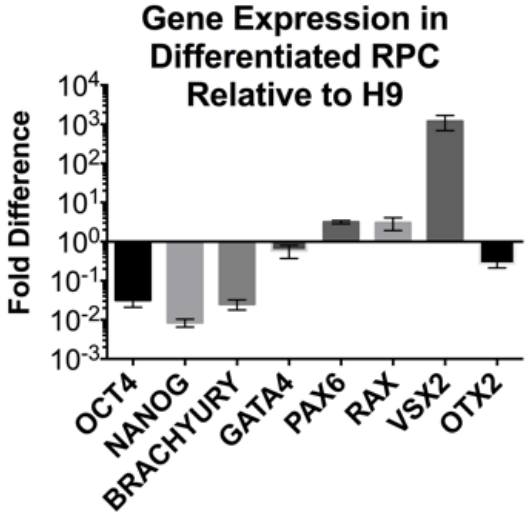

We also wanted to explore the role of the extracellular matrix compound Matrigel in promoting retinal differentiation. An experiment was performed to compare cultures incubated for one day with apical media containing 2% Matrigel, and cultures incubated for three days (Figure 9). Both cultures showed upregulation of the neural markers Pax6 and Vsx2, as well as upregulation of Crx and S-opsin. MITF was

upregulated while Otx2 was downregulated fourfold. Since MITF is required for differentiation of RPE, these data may suggest that a few of the H9-hESC cells differentiated towards RPE rather than neural retina. No gross pigmentation of the Transwell filters was observed at any point in the experiments. Regardless, these data indicate a significant population of multipotent retinal progenitor cells. A statistical analysis showed equivalent expression between cultures differentiated after one-day Matrigel and three-day Matrigel exposure. For all further experiments, cells were incubated for one day.

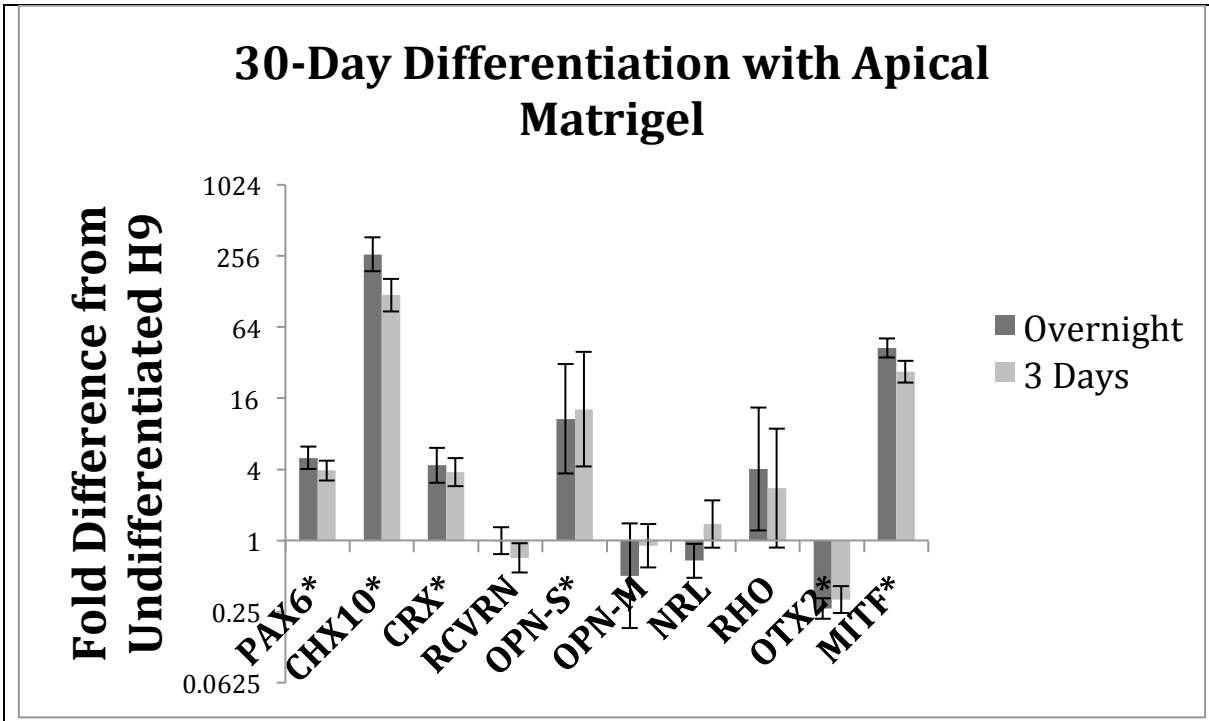

Figure 9. Comparison of overnight versus three day incubation with 2% Matrigel in N2B27 in the apical media chamber. For the remainder of the 30-day differentiation N2B27 media was used for both apical and basolateral chambers. No significant differences were observed between overnight and three-day treatment. Single experiment with PCR reactions performed in triplicate. Error reported as SEM.

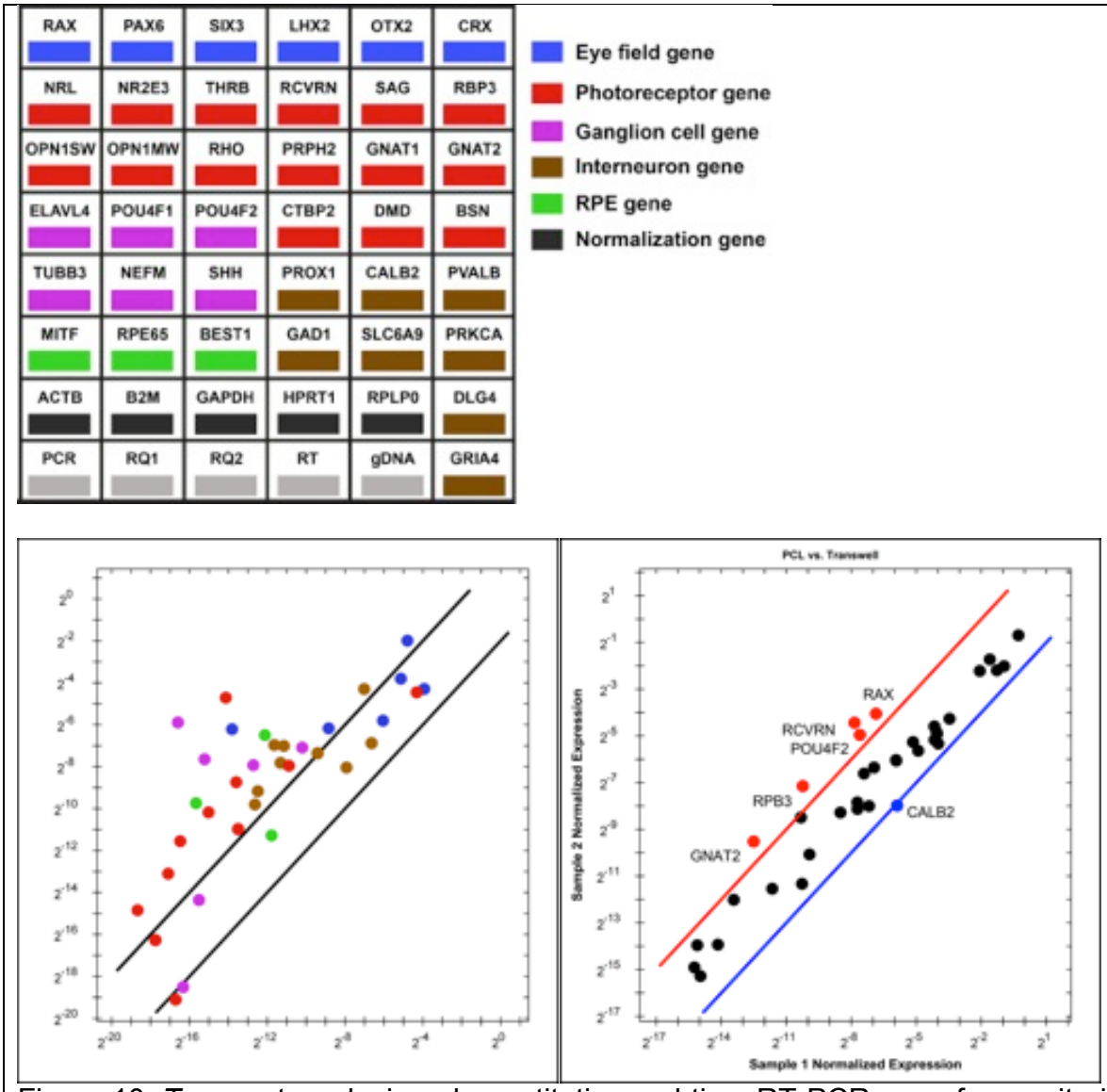

Figure 10. *Top*, custom-designed quantitative real-time RT-PCR array for monitoring and comparing maturation towards neural retina. The array contains genes of various retinal markers, including markers expressed during development (eye field, blue), in photoreceptors (red), in ganglion cells (light purple), and in bipolar, horizontal, amacrine, and Muller cells (brown). The array also contains several housekeeping genes and internal and external PCR controls. *Bottom left*, single comparative experiment of gene expression in H9-hESC differentiated on PCL scaffolds for 1 month and H9-hESC. 71% of genes were expressed more than fourfold (upper diagonal black line) compared to H9. *Bottom right*, single comparative experiment of gene expression when H9-hESC were differentiated on PCL scaffolds versus Transwell filters. Five genes were upregulated more than fourfold (red diagonal line) on PCL scaffolds compared to Transwell filters. One gene was downregulated fourfold (blue diagonal line).

A Biorad PCR array for 48 marker genes involved in differentiation and function of the neural retina was used to compare the differentiation profile of cultures grown on PCL scaffolds to undifferentiated H9-hESC and to cultures grown on Transwell filters. Relative to undifferentiated H9-hESC, differentiated cells on PCL scaffolds showed upregulation of eye field transcription factors (Rax and Pax6), photoreceptor genes (Crx, recoverin, Thrb, S-opsin, M-opsin, S-arrestin, peripherin-2, Gnat1, Gnat2, Rbp3) and interneuron genes (Elavl4, Pou4f1, Pou4f1, Prox1, Neurofilament-M, Calb2, Pvalb). Interestingly, there was minimal change in expression of rod photoreceptor genes (Nrl, Nr2e3, rhodopsin). Compared to neural retina differentiated on Transwell filters, neural retina differentiated on PCL scaffolds showed increased expression of several genes including Rax, recoverin, Gnat2, Pou4f2, and Rbp3, and minimal change in expression of other genes. These results suggest that at the transcript level, PCL scaffolds are equivalent or superior to Transwell filters for the directed differentiation of H9-hESC to neural retina.

Next, immunofluorescence staining and confocal microscopy were used to compare the tissue morphology of neural retina grown on scaffolds versus Transwell filters. On Transwell filters, some neural rosettes persisted in between areas of flattened monolayers of neural retinal cells. Figure 11 is a representative example of a junction between neural rosette and monolayer. Cells in the neural rosette were positive for Crx. Interestingly, the monolayer of this area was loosely populated with cells that were positive for cytoplasmic Prox1, showing elongated processes similar to neuronal axons. Another field showed a region containing a monolayer of $Pax6^{+}Crx^{+}$

cells. Some cells within the monolayer stained more brightly for Crx than Pax6 relative to other cells, suggesting that different cells may be at different stages of maturation.

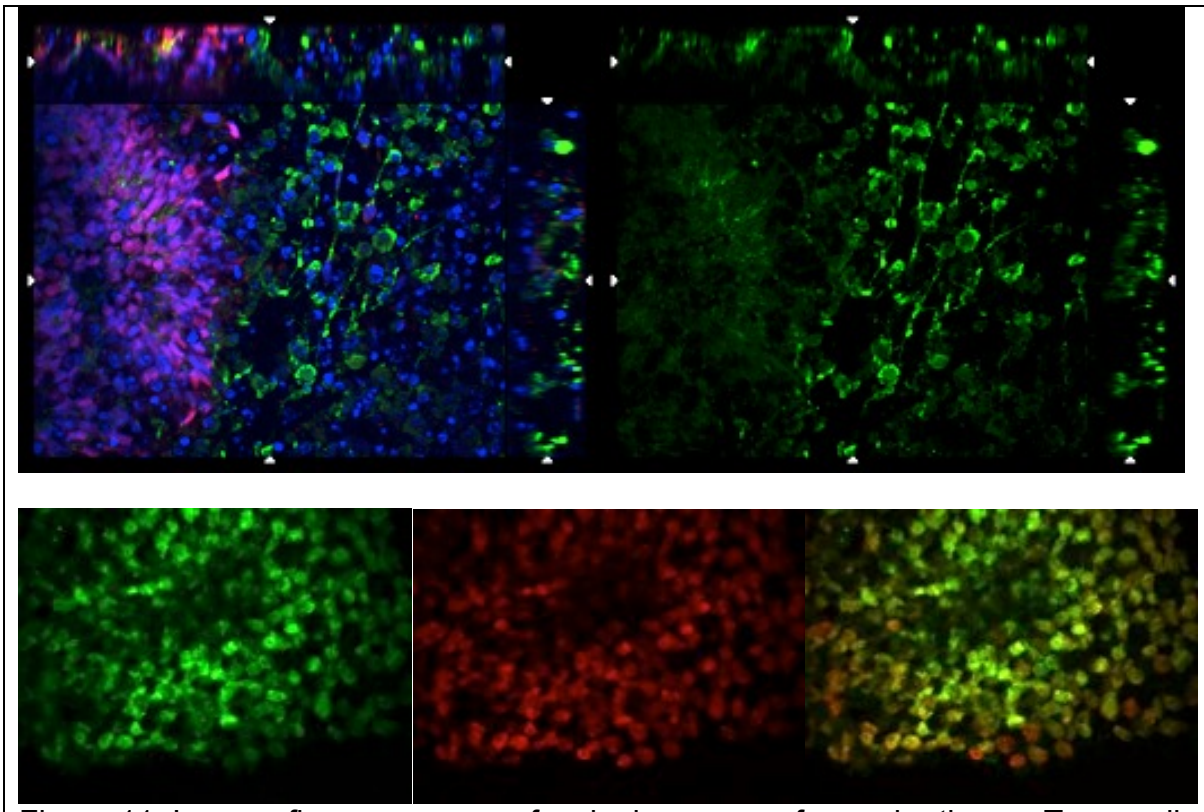

Figure 11. Immunofluorescence confocal microscopy of neural retina on Transwell filters. *Top*, example of a neural rosette with heterogeneous cell population. Crx (red) localizes to nuclei (DAPI, blue) and Prox1 (green) localizes to cytoplasm. *Bottom,* $Pax6^+$ (green) and Crx^+ cells growing as a flat monolayer.

On PCL scaffolds, staining for the proliferation marker Ki-67 and nuclear DAPI revealed both proliferating and non-proliferating cells at the scaffold surface and up to 40 microns inside the scaffold interior (Figure 12). Initially H9-hESC were seeded at the scaffold surface as colonies 200 microns in size, which is larger than the scaffold pore size of 20-40 microns. In addition individual cells within the scaffold interior could not have deposited there initially, since hESC undergo rapid apoptosis in the absence of cell aggregation [36]. Therefore it is most likely that cells successfully adhered as

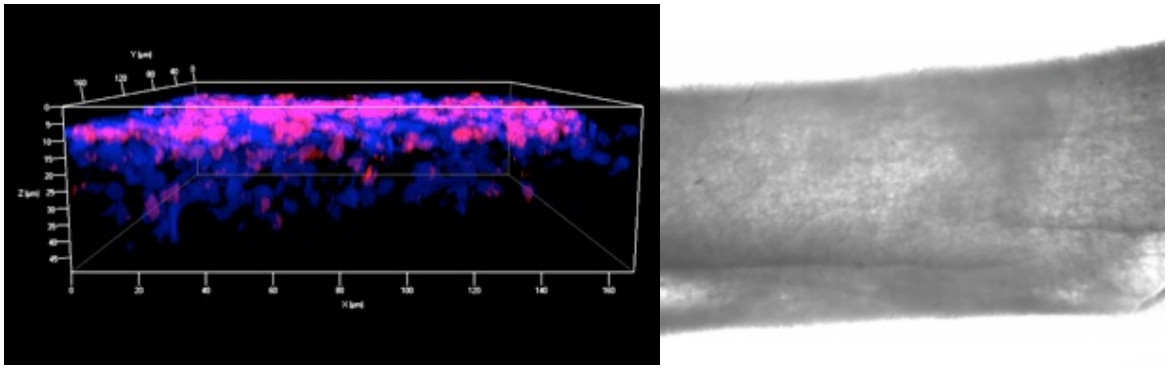

Figure 12. *Left*, Z-dimensional slice through PCL scaffold showing cell nuclei (DAPI, blue) and cell proliferation (Ki-67, red). The scaffold surface has a higher fraction of Ki-67^{+} cells. *Right*, example of scaffold curling property seen with a 100 micron thick scaffold. While H9 are able to attach to the scaffold (seen as opacities), the functional surface area is decreased and physical manipulation was technically challenging.

colonies at the scaffold surface, and then progressively migrated up to 40 microns towards the interior. We found a reduced proportion of proliferating cells at the scaffold interior, which was concerning for reduced nutrient and oxygen availability. Since the cells did not penetrate the full thickness of the scaffold, we attempted to manufacture thinner scaffolds by reducing the amount of polymer solution loaded into the syringe pump while keeping all other electrospinning parameters constant. Unfortunately, scaffolds thinner than 150 microns tended to curl up into scrolls immediately after being cut from the scaffold, a property which made cell seeding and mechanical manipulation prohibitively challenging. We initially though the curling could be due to electrostatic or hydrophobic forces, but curling could not be relieved by chemical treatment with 1M sodium hydroxide or coating with Matrigel. Curling also persisted despite application of a weighted object for several hours. We believe the curling is a mechanical artifact generated by the electrospinning process, since fibers are collected on a rotating mandrel. Further experiments were performed with scaffolds 150 microns thick, keeping the limitation of scaffold penetration in mind.

By immunofluorescence cells grown on the PCL scaffold were positive for the early retinal marker Pax6, and subpopulations of these cells were $Vsx2^{+}$, $Prox1^{+}$, and $Crx^{+}recoverin^{+}$ (Figure 13). S-opsin could not be detected despite increased mRNA expression, which suggests post-transcriptional regulation. As expected from the mRNA data rhodopsin could not be detected. Individual PCL fibers can be visualized near positively staining cells, indicating that cells can differentiate and survive near degrading PCL fibers. Overall, immunofluorescence microscopy suggests a heterogenous population of cells consistent with neural retinal identity. Taken together, the PCR and immunofluorescence data support the hypothesis that Matrigel-scaffolds allow H9-hESC cellular adhesion, migration, and proliferation while supporting differentiation to neural retina. Differentiation is incomplete at 30 days as demonstrated by the presence of many $Vsx2^{+}$ retinal progenitor cells, and some retinal cell populations are present while others may require more time to develop.

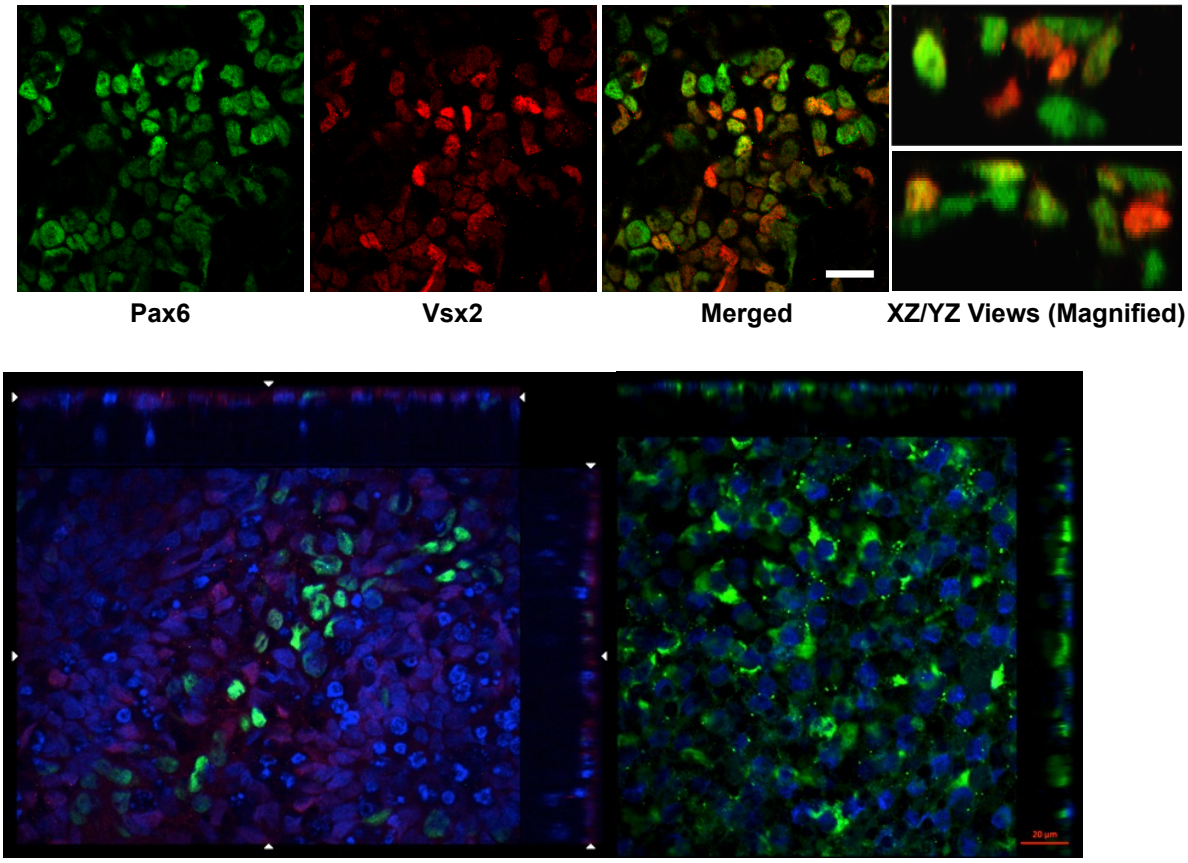

Figure 13. Immunostaining of cells differentiated on PCL scaffolds. *Top*, Scaffold permits growth of $Pax6^+$, $Vsx2^+$, and $Pax6^+Vsx2^+$ cells. PCL fibers are visible as signal voids. Z-stack imaging shows a neural retinal multilayer. *Bottom left,* one area of scaffolding showing Crx^+ (red) cells and $Prox1^+$ (green) cells with nuclear distribution of both markers. *Bottom right*, $Crx^+recoverin^+$ (Crx blue, recoverin green) photoreceptor-like cells distributed on the surface of the scaffold.

Aim 2: Assess whether hESC-derived neural retina grown on PCL can be induced to further maturity by co-culture with RPE.

Co-culture with RPE

hfRPE and H9-RPE were previously shown to adopt characteristics similar to native adult RPE in a serum-free medium (SFM-1), including expressing known RPE markers, phagocytosing photoreceptor outer segments, and maintaining barrier

function and transepithelial electrical resistance (TER). We tested whether hfRPE and H9-RPE could thrive similarly in N2B27, the medium used to differentiate neural retina. We found that both hfRPE and H9-RPE could maintain their TER for at least 1 month after the media was switched from SFM to N2B27. After 1 month, hfRPE and H9-RPE were stained for the RPE markers paracingulin and Otx2. Both hfRPE and H9-RPE continued to express paracingulin at the apical tight junction and Otx2 in the nuclei, indicating that RPE can be cultured in the same N2B27 media used to differentiate neural retina.

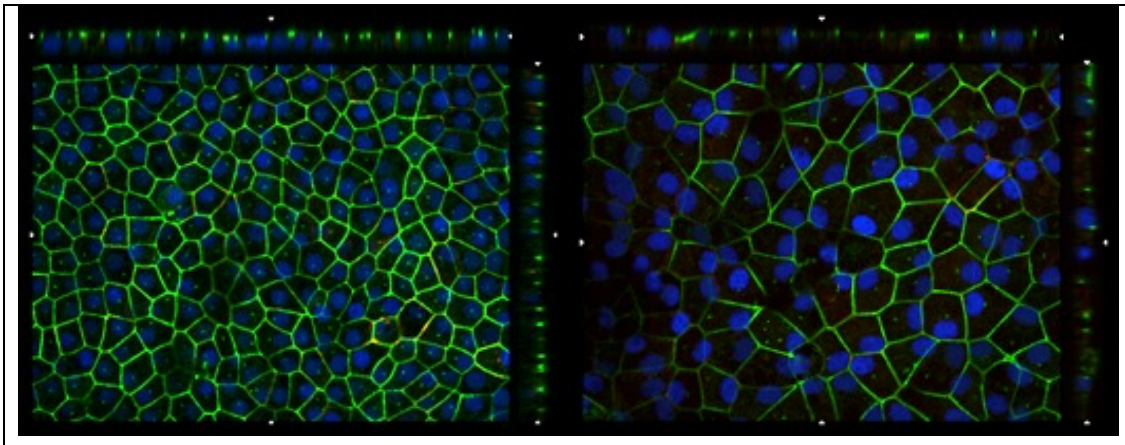

Figure 14. Immunostaining of H9-hESC derived RPE and hfRPE after being maintained in N2B27 neural differentiation media for 1 month. Both cultures retained characteristics of RPE including tight junctions (paracingulin, green), nuclear Otx2 (blue), polygonal morphology, and pigmentation (not shown).

We then sought to co-culture stem cells undergoing directed differentiation to neural retina with RPE. First, H9-hESC were seeded to PCL scaffolds and differentiated for 2-4 weeks in N2B27 media as described under results for Aim 1. Then, PCL scaffolds were flipped and transferred to the top of an RPE monolayer. Co-cultures were maintained for an additional 2-4 weeks and TER was monitored. When hfRPE was used for co-culture, within 2 days the TER value dropped from 600-1000 Ω

x cm^2 to the normal adult TER range of 200-300 Ω x cm^2, and remained in that range for the following 2-4 weeks. Control samples in which acellular scaffolds were transferred to a monolayer of RPE in the identical manner maintained the higher TER values characteristic of monocultured hfRPE. This result suggested that paracrine effects or contact with the neural retina itself exerted a modulating effect on RPE tight junctions.

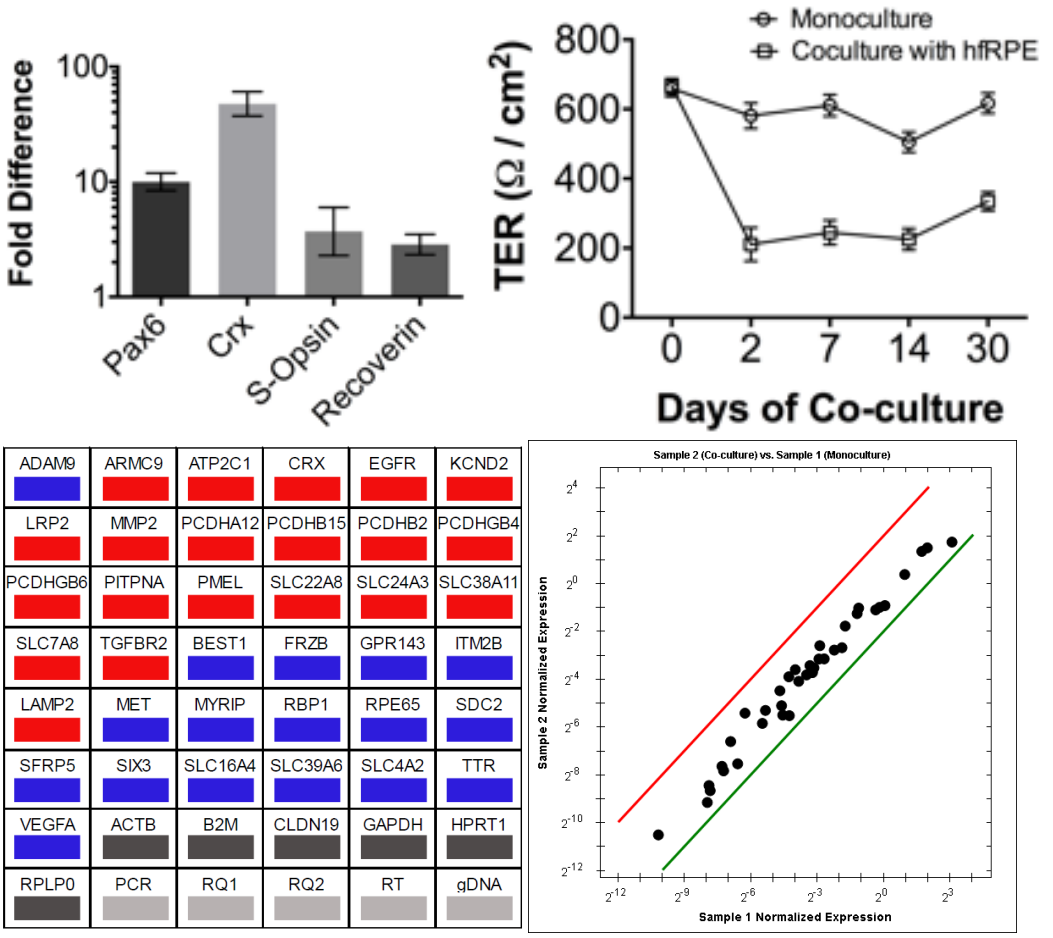

Figure 15. Co-culturing neural retina with RPE affects the maturity of both tissues. *Top left*, neural retina upregulated Pax6 and Crx as well as S-opsin and recoverin compared to monoculture. *Top right*, the TER of co-cultured hfRPE is modulated towards adult physiologic values (200-300 Ω x cm^2), whereas monoculture maintains high TER values. *Bottom*, a PCR array of genes for monitoring RPE maturation showed no significant differences in expression between monocultured and co-cultured H9-RPE.

After 2-4 weeks of co-culture the scaffold was manually separated from the RPE monolayer and the two layers were analyzed separately by immunofluorescence and qRT^2-PCR. Compared to control monocultures of neural retina, co-cultured neural retina showed greater than fourfold increase in Pax6 and Crx, and statistically significant but less than fourfold increase in recoverin and rhodopsin. Co-cultured RPE showed no changes in morphology or RPE marker expression as assessed using a PCR array of signature RPE genes, which may reflect the highly mature state of 16-week hfRPE.

Aim 3: Characterize TRP channels of the RPE and their role in regulating RPE function.

Barium Disrupts RPE Monolayers When Added to the Apical Surface

We turned our attention to the role of TRP channels in regulating intracellular [Ca^{2+}] in the RPE. Intracellular [Ca^{2+}] regulates many RPE functions including secretion of growth factors, transport of water and ions, and phagocytosis of shed photoreceptor outer segments. We explored whether TRP channels could play a role in regulating neural retina-RPE interactions.

When extracellular [Ca^{2+}] was increased from 1.3 to 6.3 mM by the addition of $CaCl_2$, the TER transiently decreased ~20% (Figure 16). Caloxin 1b1 is an inhibitor of the plasma membrane calcium-ATPase (PMCA). PMCA isoforms 1, 2 and 4 are found in human RPE [37]. With increased extracellular [Ca^{2+}] plus caloxin 1b1, the TER decreased ~40% and did not recover during the experiment. The concentration of caloxin 1b1 used in this experiment was > 3-10× the pK_i of these isoforms, which

would achieve a partial inhibition [38]. Inhibition of PMCA by itself had no effect. To explore further, we used Ba^{2+} as a surrogate for Ca^{2+}, because it is a poor substrate for PMCA and is not also transported by the smooth endoplasmic reticulum calcium-ATPase.

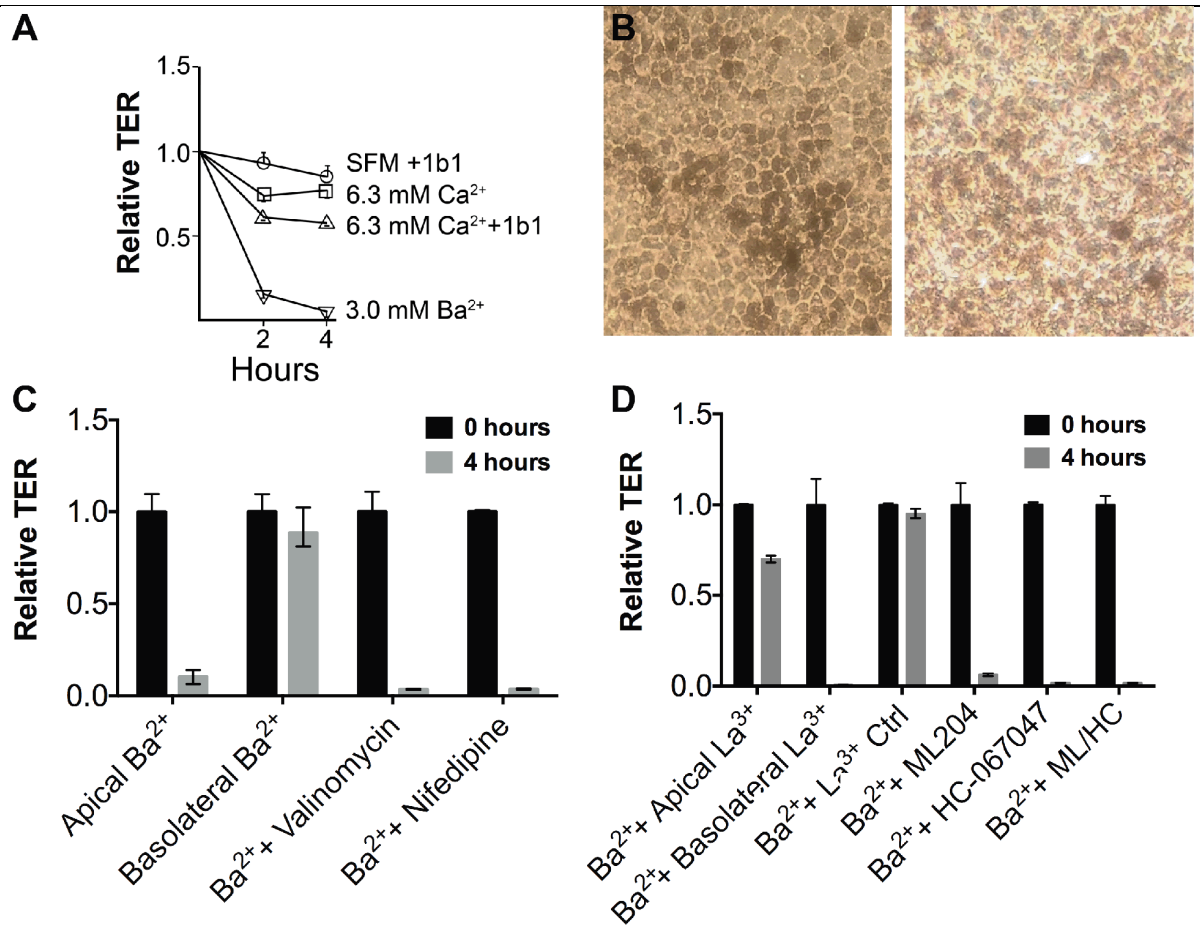

Figure 16. Effect of $BaCl_2$ on hfRPE in culture media. TER is reported relative to the TER at the start of the experiment (TER ≥ 300 Ω×cm^2). Except where noted the results are based on three independent experiments (mean±SE). (A) The results for SFM-1 and SFM-1 plus caloxin 1b1 (Ca^{2+}-ATPase inhibitor) were indistinguishable. The effect of adding $CaCl_2$ was transient with a small but significant decrease ($p<0.05$) at 2 hr. The decrease was prolonged in the presence of the inhibitor ($p<0.05$ relative to Ca^{2+} alone). $BaCl_2$ caused significant reduction of TER after two and four hours in SFM at 37°C. (B) Light microscopy revealed normal polygonal RPE morphology after 4 hours in 5 mM $CaCl_2$ (left) and loss of the apical junctional complex after 4 hours in $BaCl_2$ (right). (C) TER decreased when $BaCl_2$ was added to the apical media chamber, but not when added to the basolateral chamber

(mean±SE). Valinomycin and nifedipine were ineffective at preventing TER reduction (mean±range, n=2). (D) $LaCl_3$ in the apical chamber partially blocked the Ba^{2+}-mediated effect, but $LaCl_3$ in the basolateral chamber was ineffective. Inhibitors of TRPC4 (ML204) and TRPV4 (HC-067047), alone and in combination (ML/HC), failed to block the effect of Ba^{2+}. (mean±range, n=2). Panels C and D prepared with data obtained in part by Geliang Gan.

Barium permeates through TRP channels and can also block K^+ channels [34, 39, 40]. When 3 mM $BaCl_2$ was added to the culture medium the TER decreased substantially within 2 hours at 37°C (Figure 16). There was no discernable change in morphology and the TER recovered several days after the Ba^{2+} was washed away. By 4 hours, cells in $BaCl_2$ disassembled the apical junctional complex (adherens and tight junctions), lost polygonal morphology, and began to detach from the filter. To determine whether the Ba^{2+}-mediated effect was polarized, $BaCl_2$ was added to either the apical or basolateral medium chamber. Reduction in TER was reproduced only when Ba^{2+} was added to the apical chamber. The K^+ ionophore valinomycin was used to determine whether the effect on TER could be relieved by providing an alternative route for K^+ to exit the cell. The blocker nifedipine was used to determine whether Ba^{2+} was exerting its effect through voltage-gated L-type channels. Neither valinomycin nor nifedipine could relieve the Ba^{2+}-mediated decrease of TER. Based on these results we explored the hypothesis that Ba^{2+} may exert its effect after entering cells via TRP channels located on the apical membrane.

Lanthanum is a general TRP channel blocker [41]. At 2 mM, $LaCl_3$ reduced the ability of Ba^{2+} to lower the TER by 75% when both were added to the apical media chamber (Figure 16). In contrast, $LaCl_3$ was ineffective when only added to the basolateral chamber. The reduction in TER could not be attributed to a specific TRP channel through the use of selective inhibitors. We examined ML204, an inhibitor of activated TRPC4, [42] and HC-067047, an inhibitor of TRPV4, [43] and a combination of the two. The inhibitors were tested at concentrations 20-fold higher than their IC_{50}, but they did not block the effect of Ba^{2+} on TER.

A comprehensive view of TRP channel gene expression was obtained by consulting an RNA-sequencing database generated from previous hfRPE cultures [37]. High levels of gene expression were observed for TRPC1, TRPC4, TRPM1, TRPM3, TRPM7, and TRPV4. Using qRT^2-PCR, we verified high expression levels of these six channels, as well as reduced (100-fold less than RPE marker claudin-19), or negligible, expression of the remaining TRP channels (Figure 16). These data were consistent across multiple cultures that were isolated from distinct donors.

Immunoblots were used to characterize the expression of TRP channel proteins with high mRNA expression (Figure 17). TRPC1 protein was not detected. TRPC4 was detected near 90 kDa, in agreement with the predicted molecular weight. Three TRPM channels were visualized at molecular weights different from their predicted protein sizes, which is common for membrane proteins. TRPM1 was visualized as three bands, one near 250 kDa and two in close proximity near 125 kDa. Corresponding bands were observed in a positive control, lysates from the TRPM1-expressing cell line 501mel (Figure 17). TRPM3 was detected near 250 kDa, consistent with past studies [44]. TRPM7 was also detected near 250 kDa, consistent with sizes detected in the manufacturer's positive controls. Anti-TRPV4 antibody stained an appropriately sized protein near 90 kDa. Several other weakly stained proteins were also observed. Labeling of these bands was blocked by preincubating the antibody with the peptide antigen.

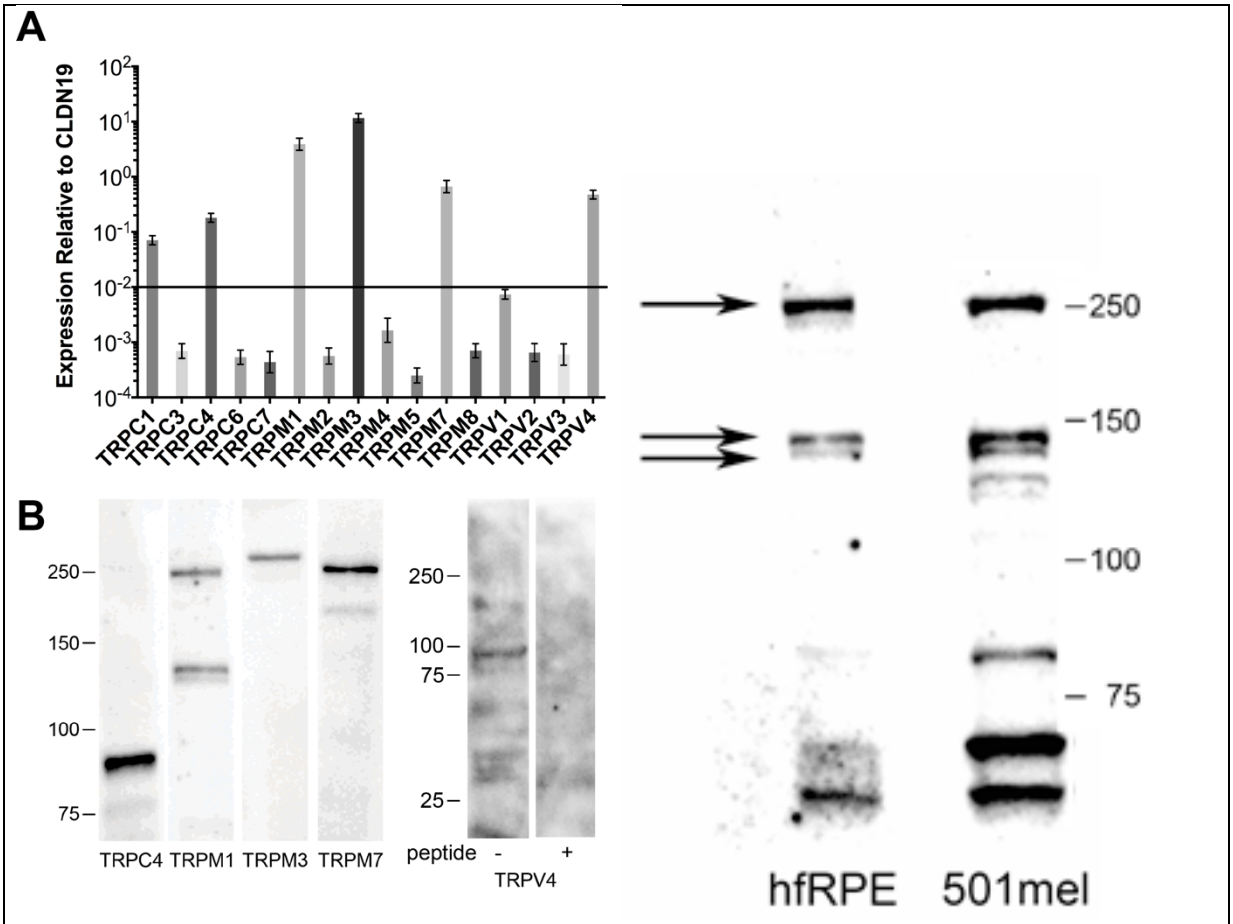

Figure 17. *Left*, expression of TRP channels in hfRPE cultures. (A) Quantitative RT-PCR showing gene expression relative to tight junction gene CLDN19. Horizontal line delineates 100-fold less expression than CLDN19. Transcripts that were undetected after 40 cycles of PCR are not included: TRPC5, TRPM6, TRPV5, TRPV6, and TRPA1. Error bars: SE, n≥3 (B) For genes that expressed high levels of mRNA, immunoblots revealed proteins of the appropriate M_r (see text). Preincubation of the anti-TRPV4 antibody with the peptide antigen prevented the labelling of TRPV4 (~90 kDa) and a several minor protein bands. *Right*, Extra protein bands for TRPM1 were also observed in immunoblots of 501mel, a cell line rich in TRPM1. Panel A prepared with the help of Geliang Gan. TRPV4 blots in Panel B prepared by Shao-bin Wang.

Immunofluorescence and confocal microscopy were used to determine the subcellular localization of TRP proteins. TRPC4 co-localized with the tight junction protein ZO-1 (Figure 18). Because Ba^{2+} caused tight junctions to dissociate, we tested the hypothesis that a localized increase of Ba^{2+} near the tight junctions might activate

calpain-mediated dissociation of the tight junctions [45, 46]. The calpain inhibitor, ALLM, slightly blocked the effect of Ba^{2+}on TER, but was less effective than La^{3+} (Figure 19).

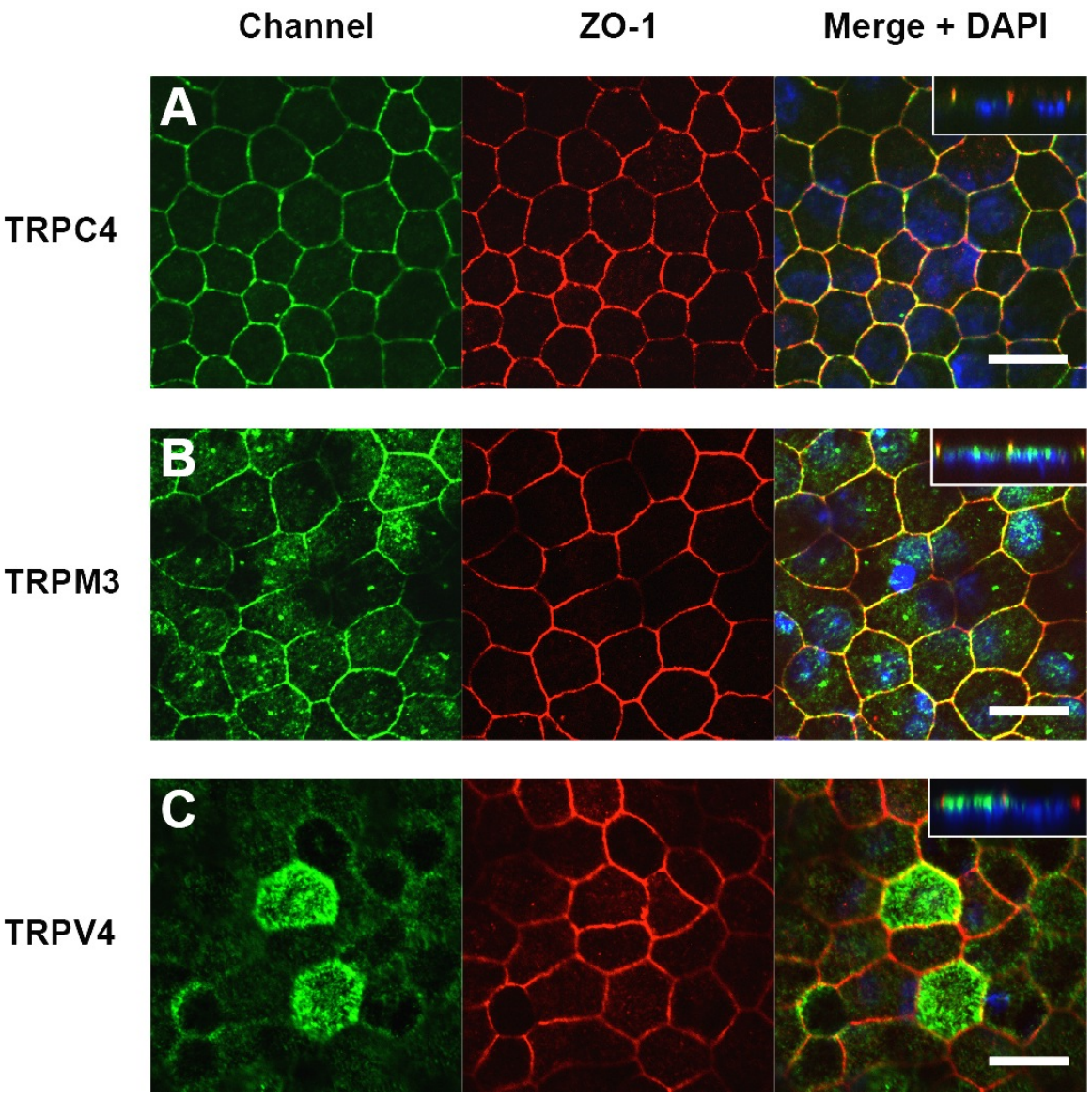

Figure 18. Subcellular localization of TRP channels by confocal immunofluorescence microscopy. In merged images, the DAPI counterstain (blue) revealed the position of nuclei. The inset shows the xz plane. (A) TRPC4 co-localized with ZO-1 in apical tight junctions. (B) TRPM3 also localized to tight junctions and to a punctate structure near the center of the cell, in the plane of the apical junctional complex. (C) An immune-signal for TRPV4, appeared in only ~5%

of cells. In positive cells, TRPV4 was observed in a punctate pattern at the apical surface that is typical of microvilli. Scale bar, 20 μm. Panels A and B courtesy of Geliang Gan.

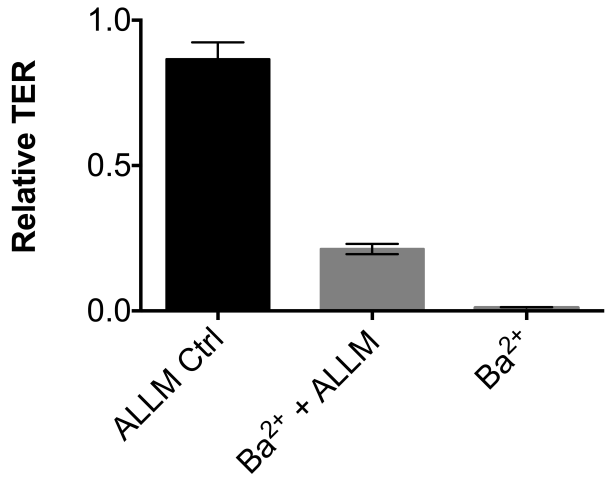

Figure 19. Calpain inhibition reduces the effect of BaCl2 on TER. Data was collected after a 2 hour incubation. TER is reported relative to the TER at the start of the experiment (TER ≥ 300 Ω×cm2). ALLM had a small, but significant, effect on the action of BaCl2 ($p < 0.001$). Error bars, SEM (n=3).

TRPM3 was concentrated in two locations along with a weaker immunofluorescence signal that corresponded to microvilli (Figure 18). An intense signal for TRPM3 co-localized with the tight junction marker ZO-1 at the apical end of the lateral membranes. TRPM3 was also concentrated at a punctate locus near the center of the cell and apical to the nucleus. This location would correspond to the basal body, which lies at the base of the primary cilium. Antibodies to γ-tubulin were used to identify the basal body [47]. At the resolution of immunofluorescence, a γ-tubulin signal would overlap with a membrane protein at the base of the cilium. Double immunolabeling with anti-TRPM3 demonstrated co-localization of the two antigens (Figure 20). The length of the primary cilium was revealed using anti-acetylated tubulin, and indicated that TRPM3 was confined to the base of the cilium.

In roughly 5% of cells, TRPV4 was observed in the punctate apical pattern typified by microvilli (Figure 18). The majority of cells showed weak staining. The immunofluorescence localization studies for TRPM1 and TRPM7 were inconclusive due to a weak, diffuse signal.

Figure 20. Localization of TRPM3 at the base of the primary cilium. The basal body, which lies at the base of the cilium was identified with antibodies to g-tubulin. The cilium was identified with antibodies to acetylated tubulin (Ac-Tubulin). The confocal image was taken above the plane of the tight junctions and shows the cilium of two adjacent cells. In one cell, the cilium was perpendicular to the plane of the image (arrowhead) and the signals for each protein overlaps. In the other cell, the cilium lies in the plane of the image. Only the g-tubulin and TRPM3 signals overlap to give an orange signal. Bar, 5 microns. Images courtesy of Shaomin Peng.

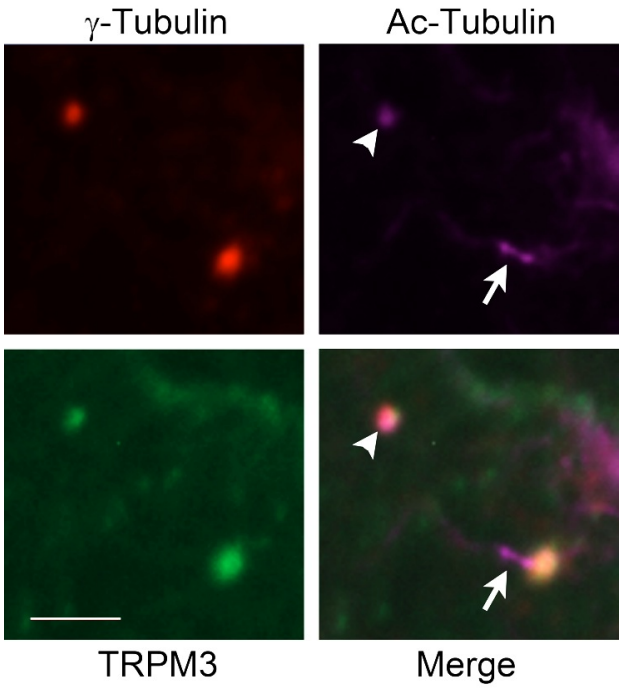

Discussion

AMD is the most common cause of elderly blindness in the developed world and patients with advanced dry AMD have no treatments available to slow progression or reverse disease. This project aimed to apply modern knowledge in tissue engineering, stem cell differentiation, and embryology towards a solution for degenerative retinal diseases including AMD. Firstly, I determined that the three-dimensional environment of an extracellular matrix-coated PCL scaffold could direct hESC to differentiate to neural retina with similar or increased efficiency as compared to conventional two-dimensional surfaces. The subsequent aim was to leverage the

embryologic interactions between neural retina and RPE by co-culturing neural retina grown on PCL scaffolds with RPE. The aim was to determine whether the co-culture model could further the maturity of either or both tissues. Finally, I examined the expression pattern of TRP channels in a model of highly mature human RPE to determine whether TRP channels could have a role in directing neural retina-RPE interactions.

Directed Differentiation and Co-culture of Neural Retina

One significant challenge was establishing a method for differentiating stem cells to neural retina. Over the past ten years the approach to differentiation has changed considerably. In 2006, Lamba and Reh first described a method of generating neural retinal cells through stimulation of the IGF pathway and inhibition the Wnt and BMP pathways using IGF-1, Dkk, and Noggin [48]. Osakada and Takahashi were able to enhance photoreceptor yield by Notch inhibition and addition of retinoic acid [49]. However, Notch inhibition caused premature exit of retinal progenitor cells from the cell cycle and retinoic acid slowed photoreceptor precursor growth. Their method yielded only 15.8% neural retinal ($Pax6^{+}Rx^{+}$) cells after 35 days, and required up to 200 days to generate photoreceptors. In 2009, Eiraku and Sasai discovered that mouse embryonic stem cells could self-organize into optic cups in free-floating culture, and Sasai's group confirmed a similar finding for hESC in 2014 [13]. Their studies also highlighted the critical role of the extracellular matrix, using dilute 1% Matrigel in the media from day 2 to day 18 to form the optic cups. Between

2010 and 2014, several other groups confirmed the self-organizing capacity of stem cells, each using slightly different methods [15, 21, 32, 35].

This project achieved directed differentiation using a protocol adapted for seeding to scaffold matrix. Matrigel, an extracellular matrix reagent containing laminins and collagens, was used to coat Transwell filters and PCL scaffolds. We found no difference between adding Matrigel to the apical culture chamber for one day versus three days, which may suggest that the most crucial contact with the appropriate extracellular matrix occurs early in differentiation. Cells were cultured in N2B27, a serum-free defined differentiation media. Our results are consistent with the literature, which shows that B27 supplement promotes neural retinal differentiation and removing B27 from the media prevents cells from attaining a retinal fate [35]. Our method allowed us to generate $Pax6^+$ cells with high yield, and subsequently $Vsx2^+$ and Crx^+ cells. On both Transwell and PCL scaffolds, there was increased gene expression for various retinal neuronal markers. Interestingly, at 30 days we observed upregulation of gene expression for S-opsin and M-opsin and minimal change in expression of Nrl, Nr2e3, or rhodopsin on both Transwell filters and PCL scaffolds, suggesting that the photoreceptor precursors in our cultures differentiated towards cones rather than rod photoreceptors. In contrast, other studies typically observe a bias towards rod photoreceptor generation [21, 49]. The reasons for this difference are not entirely clear and may be related to a differing component within our defined media, or differences in in differentiation protocol that bias photoreceptor precursors towards cone formation. The limitation of our approach to differentiation is a reliance on Matrigel, which is produced from the Engelbreth-Holm-Swarm mouse sarcoma cell line. Though

use of Matrigel may be appropriate for experiments *in vitro*, the nonhuman origin of the mixture would raise concerns about transmitting viruses or provoking an immunologic response. Availability of a human extracellular matrix component will be a crucial step in translating work in the stem cell field to the bedside.

Tissue engineered scaffolds are one method by which three-dimensional cultures may be obtained. The advantages of using a scaffold include enhanced cell survival after transplant and improved cellular adhesion. Several studies in the past have found that scaffolds of varying composition support the adhesion, migration, and differentiation of stem cells to neural retina. We chose polycaprolactone because of its nontoxicity to the retina, slow degradation, and mechanical properties. PCL scaffolds coated with Matrigel supported differentiation towards neural retina. While cells attached well to scaffolds, they could only migrate up to 40 microns into the scaffold interior, suggesting reduced availability of nutrients and/or oxygen at the scaffold interior. However, the thickness of the scaffold was appropriate to the thickness of neural retina. As a future experiment, a high-oxygen environment could be tested to see whether cells penetrate further into the scaffold, but this must be balanced with the fact that *in vivo* neural retina develops in a hypoxic environment [50]. In fact, early exposure to oxygen in premature infants causes retinopathy of prematurity. There are many adjustable scaffold properties and these properties may be instrumental in directing differentiation. For example, the Young's modulus of scaffolds can determine whether stem cells become ectoderm, mesoderm, or endoderm [51]. Lilangi Ediriwickrema's previous work confirmed that the macroscopic Young's modulus of electrospun PCL scaffolds was similar to that of native adult neural retina [52]. As a

future direction, atomic force microscopy could be performed to determine whether the mechanical properties of individual PCL fibers are suited for neuroectodermal differentiation. Newer fabrication technologies such as 3D printing may be able to create scaffold architectures with thinner individual fiber diameters to promote nutrient and oxygen entry into the inner scaffold, or create fibers that are combinations of biodegradable polymers and extracellular matrix.

Another challenge of this project was developing the framework for co-culture of neural retina and RPE. To date, the development of photoreceptor outer segments in stem cell derived neural retinal cultures has not been observed. One possible reason is that the photoreceptors require direct contact with RPE microvilli as a cue to build outer segments. We hypothesized that a co-culture of neural retina with RPE could provide the cell-to-cell and paracrine cues to further neural retinal maturity. Although we observed some positive interactions, such as upregulation of retinal gene markers and modulating of RPE TER towards physiologic values, we did not observe the formation of outer segments or outer segment-like projections in photoreceptors. Few other groups have successfully attempted to co-culture neural retina with RPE [53]. One significant difficulty was choosing a time point in the *in vitro* cultures that corresponded with *in vivo* development to initiate co-culture. For example, one study found that a growth factor secreted by RPE can inhibit stem cell growth and cause apoptosis [54]. Because we were co-culturing neural retina with relatively mature and functional RPE, we had to carefully choose to co-culture at a point in development in which neural retina would have come into contact with RPE. This time point should correlate with week 10 of *in vivo* development, when the RPE is morphologically

mature and pigmented, and when ganglion and Muller cells first appear. However, the artificial combination of neural retina and RPE may not accurately recapitulate the self-organizing embryologic phenomena observed by Eiraku and Sasai. Another possibility is that the PCL scaffold itself interferes with co-culture interactions. Scaffold fibers were 2 microns in diameter, and multiple crossing fibers could impede extension of cytoplasmic processes. In the past, Shaomin Peng had attempted to place RPCs directly on top of the RPE, and found that the RPE phagocytosed the RPCs. As mentioned above, a more refined scaffold manufacturing method such as 3D printing may be needed to elicit the formation of photoreceptor outer segments. Neural retina RPE co-culture is most likely needed to elicit outer segments as neural retinal cultures alone have not been able to achieve outer segment formation even after 200 days in culture, while cells that were transplanted and integrated into mouse retina were able to extend outer segment-like processes [14].

Calcium as a Mediator of Neural Retina-RPE Interactions

The existence of RPE-photoreceptor interactions are well established, but the precise mechanisms by which RPE senses changes in the subretinal space are unknown. To understand this aspect of RPE-neural retina co-maturation, we used a well-established model of human fetal RPE that is more mature than hESC-RPE. This study developed additional tools to monitor the maturation of hESC-RPE in co-culture.

Environmental signals regulate the functions of epithelia. The diurnal fluctuation of $[Ca^{2+}]$ in the subretinal space ($[Ca^{2+}]_{srs}$) was identified 20 years ago, [55, 56] but it remains unknown whether this fluctuation has any functional consequences. The

localization of TRP channels to microdomains of the apical membrane reopens this question. The TRP channel, PKD1L1-PKD2L1, has emerged as a potential $[Ca^{2+}]_{srs}$ sensor that localizes along the length of primary cilium of RPE cultures that were derived from a one year-old child [57, 58]. PKD1L1-PKD2L1 maintained resting $[Ca^{2+}]_{cilia}$ at least 0.4 mm higher than resting $[Ca^{2+}]_i$. Modulating $[Ca^{2+}]_{cilia}$ affected the subcellular localization of hedgehog pathway proteins. Although we failed to identify this channel in fetal-derived RPE by RNA-sequencing or qRT^2-PCR, we found that TRPM3 localized to the base of the cilium. A second microdomain for TRP channels was the tight junction. As reported in other cells, TRPM3 and TRPC4 were concentrated here [59, 60]. In this perijunctional region, a higher $[Ca^{2+}]$ might increase junction permeability by activating calpain, calmodulin, or protein kinase C. TRPV4 localized to apical microvilli in a small subset of cells. We confirmed the presence of various RPE TRP channels,[41, 61, 62] but also determined their subcellular distribution. Although the presence of spurious bands on the immunoblots might be explained by degradation products or multimer formation in SDS, their presence means the data should be viewed with caution. The data suggest that RPE might express three types of calcium sensor in the apical membrane that mediate signaling via localized changes in $[Ca^{2+}]$.

Plasma membrane TRP channels provide a constitutive leak for divalent cations to enter the cell [41, 63, 64]. To counter the constant influx of Ca^{2+}, Ca^{2+}-ATPases in the plasma membrane and organelles keep $[Ca^{2+}]_{cytoplasm}$ low. This mechanism is less effective for Ba^{2+}. The sarco/endoplasmic reticulum Ca^{2+}-ATPase does not pump Ba^{2+}, and the plasma membrane Ca^{2+}-ATPase pumps Ba^{2+} at a slower

rate than Ca^{2+} [65, 66]. A rise in [Ba^{2+}] near the tight junction might activate calpain, but not calmodulin or protein kinase C [45, 46, 67].

Barium reversibly decreased the TER within 4 hours, but only when it was added to the apical medium chamber. The effect could be blocked by La^{3+}, a non-specific inhibitor of TRP and other channels. Even with Ba^{2+} added to both media chambers, La^{3+} in the apical chamber was sufficient to block the effect of Ba^{2+}. The effect of Ba^{2+} could result from its ability to block K^+ channels, principally Kir7.1, which localizes to the apical plasma membrane. This is unlikely, because valinomycin, a K^+-specific ionophore, failed to protect RPE from Ba^{2+}. Experiments with the calpain inhibitor, ALLM, supported a partial role for Ba^{2+}-activated calpain in the decrease of TER. Evidence that Ca^{2+} could regulate RPE tight junctions comes from the observation that raising the $[Ca^{2+}]_{extracellular}$ to 6.3 mM concentration while inhibiting the plasma membrane Ca^{2+}-ATPase inhibitor decreased the TER 40%. TRP-specific inhibitors did not allow us to tie these effects to a particular channel. However, these inhibitors may not have targeted the correct isoform and some affect activity stimulated by G protein coupled receptors rather than basal activity [42]. There are additional potential functions for a tight junction associated ion sensor including signaling networks that control cell size, shape, polarity, proliferation, and apoptosis [68, 69].

A mechanism for the effect of Ba^{2+} has to explain the requirement that cells be maintained in a complete medium. Previous work from our lab showed that 3 mM $BaCl_2$ had the opposite effect of increasing the TER when the $BaCl_2$ was dissolved in a modified Ringer's solution that lacked bicarbonate [34]. In this medium, the plasma

membrane electrical resistance increases as the principal membrane transport mechanisms are inhibited. With tight junctions remaining intact, the TER approximated the resistance of the tight junctions [34, 70]. Together, these data indicate mechanisms that disassemble tight and adherens junctions requires a complete medium. When $BaCl_2$ was withdrawn from the medium after two hours the cells recovered within two days, which is consistent with the time course for junction disassembly/reassembly experiments performed in other epithelia [71].

The findings on expression of TRPV channels in RPE have been inconsistent. We found TRPV4 was found in the microvilli of a small subset of cells. Regional heterogeneity of RPE has been observed for other proteins in vivo and in culture [34, 72]. Cordeiro *et al.* found expression of TRPV1-V4 in ARPE-19 and primary donor RPE cultured in media containing 10% fetal bovine serum [61]. In contrast, Kennedy *et al.* found expression of TRPV5 and TRPV6 in primary cultures of RPE cultured in 10% fetal bovine serum plus 5% newborn calf serum [62]. Our study used hfRPE cultured in a serum-free media that promotes differentiation [31]. The contradictory literature may reflect the heterogeneity of different cell cultures, as well as differing patterns of protein expression in response to different media formulations.

Although TRPM1 was detected on immunoblots, expression could not be localized to a specific subcellular compartment. Lack of expression at the plasma membrane is consistent with prior studies [73]. TRPM7 was also undetected by immunofluorescence microscopy despite its detection by immunoblotting. In vascular endothelial cells, TRPM7 channels localize to the plasma membrane in the presence

of laminar fluid flow [74]. In the absence of a stimulus, TRPM7 might be diffusely localized in an internal pool.

The hfRPE used in this study are highly differentiated and used within one passage since their isolation from 15-16 week gestation fetuses [28, 29]. Therefore the selective pressure to adapt phenotype to culture conditions has been minimized, but this also means that our cultures represent a snapshot of development. In rodents, RPE's primary cilium is transiently present during development and is involved in the differentiation of photoreceptors [75, 76]. In humans, photoreceptors differentiate during the fifth month of gestation [8]. This study identified all the TRP channels that are expressed by RPE at an earlier stage of human fetal development. It is limited by the availability and quality of antibodies and specific inhibitors. Further, TER is but one function of tight junctions that might be affected by a Ca^{2+} sensor. Given these limitations, our data indicate that TRP channels are polarized to the apical plasma membrane where they may monitor $[Ca^{2+}]_{SRS}$. Future directions for this work will include examining whether mechanical and environmental stimuli can modulate various RPE functions through their action on these TRP channels.

Conclusion

This study established a directed differentiation protocol for neural retina on PCL scaffolds and explored tissue interactions between neural retina and RPE as steps towards translating ongoing research in stem cell biology and tissue engineering towards clinical applications such as neural retinal-RPE co-transplantation. We found that H9-hESC can be directed to differentiate to neural retina using Matrigel and N2B27 neural differentiation media. PCL scaffolds permit the adhesion and migration of H9-hESC and daughter cells, and are equivalent or slightly superior to Transwell filters in supporting differentiation. Co-culturing neural retina grown on PCL scaffolds with the RPE increases the maturity of both tissues to a limited degree, and further study is needed to determine the optimal combination of a scaffold manufacturing process and a neural differentiation method, as well as optimal timing of co-culture. TRPC4, TRPM3, and TRPV4 are the TRP channels expressed in highly mature hfRPE and localize to subdomains of the RPE apical membrane, where they may contribute to Ca^{2+} sensing and regulation of various RPE functions at the primary cilium, RPE microvilli, and RPE tight junctions.

References

1. Takahashi, K. and S. Yamanaka, *Induction of pluripotent stem cells from mouse embryonic and adult fibroblast cultures by defined factors.* Cell, 2006. **126**(4): p. 663-76.
2. Friedman, D.S., et al., *Prevalence of age-related macular degeneration in the United States.* Arch Ophthalmol, 2004. **122**(4): p. 564-72.
3. Brody, B.L., et al., *Depression, visual acuity, comorbidity, and disability associated with age-related macular degeneration.* Ophthalmology, 2001. **108**(10): p. 1893-900; discussion 1900-1.
4. Heier, J.S., et al., *Intravitreal aflibercept (VEGF trap-eye) in wet age-related macular degeneration.* Ophthalmology, 2012. **119**(12): p. 2537-48.
5. Rosenfeld, P.J., et al., *Ranibizumab for neovascular age-related macular degeneration.* N Engl J Med, 2006. **355**(14): p. 1419-31.
6. Age-Related Eye Disease Study 2 Research, G., *Lutein + zeaxanthin and omega-3 fatty acids for age-related macular degeneration: the Age-Related Eye Disease Study 2 (AREDS2) randomized clinical trial.* JAMA, 2013. **309**(19): p. 2005-15.
7. Strauss, O., *The retinal pigment epithelium in visual function.* Physiol Rev, 2005. **85**(3): p. 845-81.
8. Barishak, Y.R., *Embryology of the eye and its adnexa*. 2nd rev. ed. 2001, Basel ; New York: Karger. 132 p.
9. Arroyo, J.G., et al., *Photoreceptor apoptosis in human retinal detachment.* Am J Ophthalmol, 2005. **139**(4): p. 605-10.
10. Allikmets, R., et al., *A photoreceptor cell-specific ATP-binding transporter gene (ABCR) is mutated in recessive Stargardt macular dystrophy.* Nat Genet, 1997. **15**(3): p. 236-46.
11. Schwartz, S.D., et al., *Embryonic stem cell trials for macular degeneration: a preliminary report.* Lancet, 2012. **379**(9817): p. 713-20.
12. da Cruz, L., et al., *RPE transplantation and its role in retinal disease.* Progress in Retinal and Eye Research, 2007. **26**(6): p. 598-635.
13. Nakano, T., et al., *Self-formation of optic cups and storable stratified neural retina from human ESCs.* Cell Stem Cell, 2012. **10**(6): p. 771-85.
14. Gonzalez-Cordero, A., et al., *Photoreceptor precursors derived from three-dimensional embryonic stem cell cultures integrate and mature within adult degenerate retina.* Nat Biotechnol, 2013. **31**(8): p. 741-7.
15. Meyer, J.S., et al., *Optic vesicle-like structures derived from human pluripotent stem cells facilitate a customized approach to retinal disease treatment.* Stem Cells, 2011. **29**(8): p. 1206-18.
16. Redenti, S., et al., *Retinal tissue engineering using mouse retinal progenitor cells and a novel biodegradable, thin-film poly(e-caprolactone) nanowire scaffold.* J Ocul Biol Dis Infor, 2008. **1**(1): p. 19-29.
17. Tomita, M., et al., *Biodegradable polymer composite grafts promote the survival and differentiation of retinal progenitor cells.* Stem Cells, 2005. **23**(10): p. 1579-88.
18. Tao, S., et al., *Survival, migration and differentiation of retinal progenitor cells transplanted on micro-machined poly(methyl methacrylate) scaffolds to the subretinal space.* Lab Chip, 2007. **7**(6): p. 695-701.

19. Lavik, E.B., et al., *Fabrication of degradable polymer scaffolds to direct the integration and differentiation of retinal progenitors.* Biomaterials, 2005. **26**(16): p. 3187-96.
20. Yao, J., et al., *Enhanced differentiation and delivery of mouse retinal progenitor cells using a micropatterned biodegradable thin-film polycaprolactone scaffold.* Tissue Eng Part A, 2014.
21. Boucherie, C., et al., *Brief report: self-organizing neuroepithelium from human pluripotent stem cells facilitates derivation of photoreceptors.* Stem Cells, 2013. **31**(2): p. 408-14.
22. Lu, B., et al., *Long-term safety and function of RPE from human embryonic stem cells in preclinical models of macular degeneration.* Stem Cells, 2009. **27**(9): p. 2126-35.
23. Lamba, D.A., J. Gust, and T.A. Reh, *Transplantation of human embryonic stem cell-derived photoreceptors restores some visual function in Crx-deficient mice.* Cell Stem Cell, 2009. **4**(1): p. 73-9.
24. Radtke, N.D., et al., *Vision change after sheet transplant of fetal retina with retinal pigment epithelium to a patient with retinitis pigmentosa.* Arch Ophthalmol, 2004. **122**(8): p. 1159-65.
25. McUsic, A.C., D.A. Lamba, and T.A. Reh, *Guiding the morphogenesis of dissociated newborn mouse retinal cells and hES cell-derived retinal cells by soft lithography-patterned microchannel PLGA scaffolds.* Biomaterials, 2012. **33**(5): p. 1396-405.
26. Eberle, D., et al., *Outer segment formation of transplanted photoreceptor precursor cells.* PLoS One, 2012. **7**(9): p. e46305.
27. Bartsch, U., et al., *Retinal cells integrate into the outer nuclear layer and differentiate into mature photoreceptors after subretinal transplantation into adult mice.* Exp Eye Res, 2008. **86**(4): p. 691-700.
28. Peng, S., et al., *Engineering a blood-retinal barrier with human embryonic stem cell-derived retinal pigment epithelium: transcriptome and functional analysis.* Stem Cells Transl Med, 2013. **2**(7): p. 534-44.
29. Maminishkis, A., et al., *Confluent monolayers of cultured human fetal retinal pigment epithelium exhibit morphology and physiology of native tissue.* Invest. Ophthalmol. Vis. Sci., 2006. **47**(8): p. 3612-3624.
30. Gamm, D.M., et al., *A novel serum-free method for culturing human prenatal retinal pigment epithelial cells.* Invest Ophthalmol Vis Sci, 2008. **49**(2): p. 788-99.
31. Peng, S., et al., *Claudin-19 and the barrier properties of the human retinal pigment epithelium.* Invest. Ophthalmol. Vis. Sci., 2011. **52**: p. 1392-1403.
32. Zhu, Y., et al., *Three-dimensional neuroepithelial culture from human embryonic stem cells and its use for quantitative conversion to retinal pigment epithelium.* PLoS One, 2013. **8**(1): p. e54552.
33. Idelson, M., et al., *Directed differentiation of human embryonic stem cells into functional retinal pigment epithelium cells.* Cell Stem Cell, 2009. **5**(4): p. 396-408.
34. Peng, S., et al., *Effects of proinflammatory cytokines on the claudin-19 rich tight junctions of human retinal pigment epithelium.* Invest. Ophthalmol. Vis. Sci., 2012. **53**(8): p. 5016-5028.
35. Mellough, C.B., et al., *Efficient stage-specific differentiation of human pluripotent stem cells toward retinal photoreceptor cells.* Stem Cells, 2012. **30**(4): p. 673-86.

36. Watanabe, K., et al., *A ROCK inhibitor permits survival of dissociated human embryonic stem cells.* Nat Biotechnol, 2007. **25**(6): p. 681-6.
37. Rizzolo, L.J., et al. *Comparison of stem-cell derived retinal pigment epithelia (RPE) with human fetal retina pigment epithelium*. Gene Expression Ominbus 2013 Sept. 2014].
38. Pande, J., et al., *Aortic smooth muscle and endothelial plasma membrane Ca2+ pump isoforms are inhibited differently by the extracellular inhibitor caloxin 1b1.* Am. J. Physiol. Cell Physiol., 2006. **290**(5): p. C1341-C1349.
39. Owsianik, G., et al., *Permeation and selectivity of TRP channels.* Annu Rev Physiol, 2006. **68**: p. 685-717.
40. Zagranichnaya, T.K., X. Wu, and M.L. Villereal, *Endogenous TRPC1, TRPC3, and TRPC7 proteins combine to form native store-operated channels in HEK-293 cells.* J Biol Chem, 2005. **280**(33): p. 29559-69.
41. Wimmers, S. and O. Strauss, *Basal calcium entry in retinal pigment epithelial cells is mediated by TRPC channels.* Invest Ophthalmol Vis Sci, 2007. **48**(12): p. 5767-72.
42. Miller, M., et al., *Identification of ML204, a novel potent antagonist that selectively modulates native TRPC4/C5 ion channels.* J Biol Chem, 2011. **286**(38): p. 33436-46.
43. Everaerts, W., et al., *Inhibition of the cation channel TRPV4 improves bladder function in mice and rats with cyclophosphamide-induced cystitis.* Proc. Natl. Acad. Sci. U. S. A., 2010. **107**(44): p. 19084-9.
44. Lambert, S., et al., *Transient receptor potential melastatin 1 (TRPM1) is an ion-conducting plasma membrane channel inhibited by zinc ions.* J Biol Chem, 2011. **286**(14): p. 12221-33.
45. Bozym, R.A., et al., *Calcium signals and calpain-dependent necrosis are essential for release of coxsackievirus B from polarized intestinal epithelial cells.* Mol. Biol. Cell, 2011. **22**(17): p. 3010-3021.
46. Su, L.-T., et al., *TRPM7 Regulates Cell Adhesion by Controlling the Calcium-dependent Protease Calpain.* J. Biol. Chem., 2006. **281**(16): p. 11260-11270.
47. Rizzolo, L.J. and H.C. Joshi, *Apical orientation of the microtubule organizing center and associated γ-tubulin during the polarization of the retinal pigment epithelium in vivo.* Dev. Biol., 1993. **157**: p. 147-156.
48. Lamba, D.A., et al., *Efficient generation of retinal progenitor cells from human embryonic stem cells.* Proc Natl Acad Sci U S A, 2006. **103**(34): p. 12769-74.
49. Osakada, F., et al., *Toward the generation of rod and cone photoreceptors from mouse, monkey and human embryonic stem cells.* Nat Biotechnol, 2008. **26**(2): p. 215-24.
50. Bae, D., et al., *Hypoxia enhances the generation of retinal progenitor cells from human induced pluripotent and embryonic stem cells.* Stem Cells Dev, 2012. **21**(8): p. 1344-55.
51. Zoldan, J., et al., *The influence of scaffold elasticity on germ layer specification of human embryonic stem cells.* Biomaterials, 2011. **32**(36): p. 9612-21.
52. Wollensak, G. and E. Spoerl, *Biomechanical characteristics of retina.* Retina, 2004. **24**(6): p. 967-70.
53. Rodriguez-Crespo, D., et al., *Triple-layered mixed co-culture model of RPE cells with neuroretina for evaluating the neuroprotective effects of adipose-MSCs.* Cell Tissue Res, 2014. **358**(3): p. 705-16.

54. Kanemura, H., et al., *Pigment epithelium-derived factor secreted from retinal pigment epithelium facilitates apoptotic cell death of iPSC.* Sci Rep, 2013. **3**: p. 2334.
55. Gallemore, R.P., et al., *Calcium gradients and light-evoked calcium changes outside rods in the intact cat retina.* Vis. Neurosci., 1994. **11**(4): p. 753-761.
56. Li, J.D., et al., *Light-dependent hydration of the space surrounding photoreceptors in chick retina.* Invest. Ophthalmol. Vis. Sci., 1994. **35**(6): p. 2700-2711.
57. Matsunaga, H., et al., *Beta-galactosidase histochemistry and telomere loss in senescent retinal pigment epithelial cells.* Invest. Ophthalmol. Vis. Sci., 1999. **40**(1): p. 197-202.
58. Bodnar, A.G., et al., *Extension of Life-Span by Introduction of Telomerase into Normal Human Cells.* Science, 1998. **279**(5349): p. 349-352.
59. Song, X., et al., *Canonical transient receptor potential channel 4 (TRPC4) co-localizes with the scaffolding protein ZO-1 in human fetal astrocytes in culture.* Glia, 2005. **49**(3): p. 418-29.
60. Graziani, A., et al., *Cell-cell contact formation governs Ca2+ signaling by TRPC4 in the vascular endothelium: evidence for a regulatory TRPC4-beta-catenin interaction.* J Biol Chem, 2010. **285**(6): p. 4213-23.
61. Cordeiro, S., et al., *Heat-sensitive TRPV channels in retinal pigment epithelial cells: regulation of VEGF-A secretion.* Invest Ophthalmol Vis Sci, 2010. **51**(11): p. 6001-8.
62. Kennedy, B.G., et al., *Expression of transient receptor potential vanilloid channels TRPV5 and TRPV6 in retinal pigment epithelium.* Mol Vis, 2010. **16**: p. 665-75.
63. Schulz, H.L., et al., *Identifying differentially expressed genes in the mammalian retina and the retinal pigment epithelium by suppression subtractive hybridization.* Cytogenet Genome Res, 2004. **106**(1): p. 74-81.
64. Oberwinkler, J., et al., *Alternative splicing switches the divalent cation selectivity of TRPM3 channels.* J Biol Chem, 2005. **280**(23): p. 22540-8.
65. Heaps, C.L., et al., *Sarcoplasmic reticulum Ca(2+) uptake is impaired in coronary smooth muscle distal to coronary occlusion.* Am. J. Physiol. Heart Circ. Physiol., 2001. **281**(1): p. H223-H231.
66. Makani, S. and M. Chesler, *Barium Plateau Potentials of CA1 Pyramidal Neurons Elicit All-or-None Extracellular Alkaline Shifts Via the Plasma Membrane Calcium ATPase.* J Neurophysiol., 2010. **104**(3): p. 1438-1444.
67. Chao, S.H., et al., *Activation of calmodulin by various metal cations as a function of ionic radius.* Mol. Pharmacol., 1984. **26**(1): p. 75-82.
68. Steed, E., M.S. Balda, and K. Matter, *Dynamics and functions of tight junctions.* Trends in Cell Biology, 2010. **20**(3): p. 142-149.
69. Mellman, I. and W.J. Nelson, *Coordinated protein sorting, targeting and distribution in polarized cells.* Nat. Rev. Mol. Cell Biol., 2008. **9**(11): p. 833-845.
70. Reuss, L., *Epithelial transport*, in *Handbook of Physiology Section 14: Cell Physiology*, J.F. Hoffman and J.D. Jamieson, Editors. 1997, Oxford University Press: New York. p. 309-388.
71. Denker, B.M. and S.K. Nigam, *Molecular structure and assembly of the tight junction.* Am. J. Physiol., 1998. **274**: p. F1-9.
72. Burke, J.M. and L.M. Hjelmeland, *Mosaicism of the retinal pigment epithelium: seeing the small picture.* Mol. Interv., 2005. **5**(4): p. 241-249.

73. Oancea, E., et al., *TRPM1 Forms Ion Channels Associated with Melanin Content in Melanocytes*. Vol. 2. 2009. ra21-ra21.
74. Oancea, E., J.T. Wolfe, and D.E. Clapham, *Functional TRPM7 channels accumulate at the plasma membrane in response to fluid flow.* Circ Res, 2006. **98**(2): p. 245-53.
75. Delling, M., et al., *Primary cilia are specialized calcium signalling organelles.* Nature, 2013. **504**(7479): p. 311-4.
76. Nishiyama, K., et al., *Claudin localization in cilia of the retinal pigment epithelium.* Anat. Rec., 2002. **267**(3): p. 196-203.